Biochemistry

Article

Cite This: *Biochemistry* 2019, 58, 1596−1615

pubs.acs.org/biochemistry

Investigating Substrate Analogues for Mycobacterial MenJ: Truncated and Partially Saturated Menaquinones

Jordan T. Koehn,[†] Cheryle N. Beuning,[†] Benjamin J. Peters,[†] Sara K. Dellinger,[†] Cameron Van Cleave,[†] Dean C. Crick,[‡,§] and Debbie C. Crans*[,†,‡]

[†]Chemistry Department, [‡]Cell and Molecular Biology Program, and [§]Microbiology, Immunology, and Pathology Department, Colorado State University, Fort Collins, Colorado 80523, United States

Supporting Information

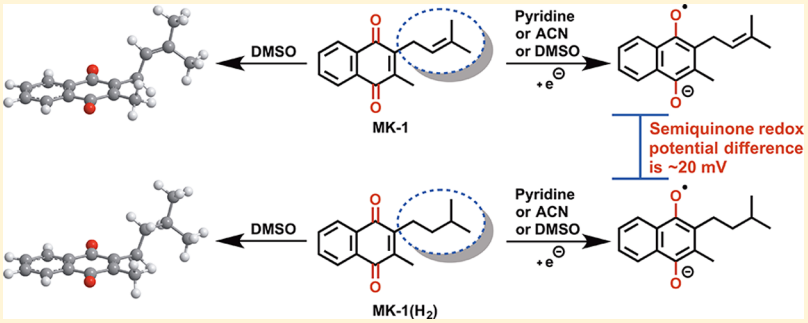

ABSTRACT: Menaquinones (MKs) are essential for electron transport in prokaryotes, and importantly, partially saturated MKs represent a novel virulence factor. However, little is known regarding how the degree of saturation in the isoprenyl side chain influences conformation or quinone redox potential. MenJ is an enzyme that selectively reduces the second isoprene unit on MK-9 and is contextually essential for the survival of *Mycobacterium tuberculosis* in J774A.1 macrophage-like cells, suggesting that MenJ may be a conditional drug target for pathogenic mycobacteria. Therefore, fundamental information about the properties of this system is important, and we synthesized the simplest MKs, unsaturated MK-1 and the saturated analogue, MK-1(H_2). Using two-dimensional nuclear magnetic resonance spectroscopy, we established that MK-1 and MK-1(H_2) adopted similar folded−extended conformations (i.e., the isoprenyl side chain folds upward) in each solvent examined but the folded−extended conformations differed slightly between organic solvents. Saturation of the isoprenyl side chain slightly altered the MK-1 analogue conformation in each solvent. We used molecular mechanics to illustrate the MK-1 analogue conformations. The measured quinone redox potentials of MK-1 and MK-1(H_2) differed between organic solvents (presumably due to differences in dielectric constants), and remarkably, an ∼20 mV semiquinone redox potential difference was observed between MK-1 and MK-1(H_2) in pyridine, acetonitrile, and dimethyl sulfoxide, demonstrating that the degree of saturation in the isoprenyl side chain of MK-1 influences the quinone redox potential. Finally, MK-1 and MK-1(H_2) interacted with Langmuir phospholipid monolayers and Aerosol-OT reverse micelle (RM) model membrane interfaces, where MK-1 adopted a slightly different folded conformation within the RM model membrane interface.

Quinones are a unique type of α,β-unsaturated ketone existing as metabolites in numerous pathways where they have many functions in nature.[1−6] The importance of quinone chemistry has been recognized since the mid-1800s. Quinone-containing compounds can be antioxidants, antitumoral agents, or carcinogenic agents and are the inherent components of biological systems such as photosystem II.[1−6] Menaquinones (MKs) (or naphthoquinones) are members of the lipoquinone (lipid-quinone) class of molecules and are essential components of the respiratory electron transport system (ETS), where they shuttle electrons and protons between protein complexes by acting as electron donors and acceptors.[6] Partial saturation of the isoprenyl side chain of MK has been known for a long time, but MenJ was recently shown to selectively reduce MK-9 at the second isoprene unit, demonstrating the origin and necessity of partially saturated MKs for the survival of the bacteria.[7,8] Currently, little is known regarding the conformation of MKs in solution or within cell membranes and how partial saturation of the isoprenyl side chain affects conformation and quinone reactivity, even though the structures and biological significance of lipoquinones and isoprenoids have been known for more than 50 years.[6,9−13] It is well-known that evolutionarily conserved structural differences in the lipoquinone headgroup alter quinone redox potential,[1] but how partial saturation of the isoprenyl side chain affects quinone redox potential remains uncertain. Therefore, this work aims to characterize the conformation of the most fundamental MKs containing

Received: January 3, 2019
Revised: February 19, 2019
Published: February 21, 2019

DOI: 10.1021/acs.biochem.9b00007
Biochemistry 2019, 58, 1596−1615

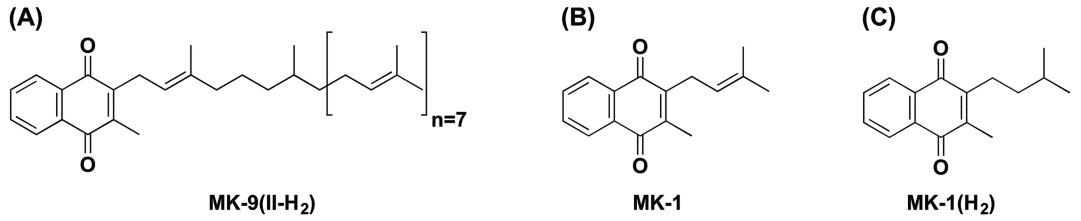

Figure 1. Structures of (A) MK-9(II-H_2), present within *Mycobacterium tuberculosis*, (B) the unsaturated MK analogue, MK-1, and (C) the saturated MK analogue, MK-1(H_2).

one isoprene unit (unsaturated vs saturated side chain) in an organic solution and a model membrane interface and to determine the quinone redox potentials of unsaturated MK-1 and saturated MK-1(H_2) in organic solutions.

MKs are structurally characterized by a naphthoquinone moiety and a repeating isoprenyl side chain of varying length (Figure 1), where the latter is a characteristic that has long been used to assist taxonomic efforts.[14,15] The most widely known MK compound is vitamin K_2 (or MK-4), which is essential for life in humans as it is a key cofactor in blood coagulation.[16] MK-4 was recently shown to be biosynthesized in humans[17] and as a part of the ETS in *Drosophila*.[18] Vitamin K_3 (or menadione), the simplest 1,4-naphthoquinone derivative lacking the isoprenyl side chain, has been reported to have significant antitumoral properties.[2] N-Alkylated MK derivatives have also been synthesized and characterized in the literature, with several exhibiting interesting biological properties.[19−22] The truncated MK analogues, menaquinone-1 (MK-1) and menaquinone-1(H_2) [MK-1(H_2)], are vital to study as they are the simplest, most fundamental MKs, where they retain the core requirements (i.e., a naphthoquinone moiety and a one-unit isoprenyl side chain). MK-1(H_2) is crucial to study as it lacks the double bond in the isoprenyl side chain, and importantly, biologically isolated MK analogues containing partial saturation (reduced double bond) in the isoprenyl side chain have been reported (Figure 1).[6−8] Truncated MK analogues are more soluble than the natural MK substrate, thus allowing rigorous characterization in aqueous assays.[8] Furthermore, MK-9 contains 80 hydrogens with significant spectral overlap, making conformational analysis nontrivial. Therefore, the conformational analysis of these two truncated MK-1 analogues is essential as the conformation of the first isoprene unit will influence the conformation of the rest of the isoprenyl side chain in naturally occurring longer MK analogues [e.g., MK-4, MK-9, or MK-9(II-H_2) (Figure 1)].

The synthesis of truncated MK analogues is necessary as it allows experimental conformational analysis to be carried out. Molecular conformations are significant for manifesting physical and chemical reactivity as well as recognition in biological systems. MKs contain alkyl side chains of varying lengths, and conformations have been reported for various alkanes, alkenes, and fatty acids, which all contain alkyl chains of varying lengths.[23−35] For example, the degree of folding of C_5−C_{32} *n*-alkanes in solution depends on the strength of the dispersion force of the solvent and increases with an increase in chain length.[27−29] Furthermore, studies of *n*-hexane and *n*-pentane in various solvents suggested that the solvent environment had only minor effects on the conformational equilibrium.[35] Interestingly, conformations observed in polar and spherical solvents such as dimethyl sulfoxide (DMSO) favored *gauche* conformations.[35] Computational studies have been carried out on MK analogues in which folded conformations were found to be favorable.[34,36] Importantly, we recently reported that menaquinone-2 (MK-2) adopts a folded, U-shaped conformation in solution and within a model membrane interface.[37] However, MK-1 contains only one isoprene unit and presents the best opportunity for a flat−extended conformation to exist, and therefore, it is important to determine if a flat−extended (i.e., trans or extended configuration of the side chain and isoprene planar), folded−extended (i.e., isoprene folded upward), or U-shaped conformation (i.e., isoprene folded up and back toward the naphthoquinone in a U shape) is preferred (see the illustration below). On the basis of these selected examples, we hypothesized that MK-1 analogues adopt folded conformations regardless of the degree of saturation in their isoprenyl side chain.

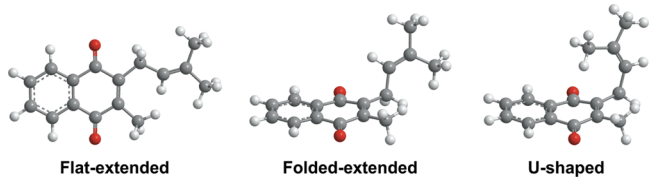

The conformation and electronic properties of a molecule can affect both the reactivity and function of a molecule in solution and within biological environments. The longer partially saturated isoprenyl side chain MK analogue, MK-9(II-H_2) (Figure 1), is an electron transporter within *Mycobacterium tuberculosis*, and the synthesis of MK-9(II-H_2) was found to be essential for the survival of pathogenic *M. tuberculosis* in host macrophages; thus, partially saturated MKs represent a novel virulence factor.[7,8] In addition, partially saturated MK analogues have been reported in other organisms such as members of the genera *Streptomyces* and *Actinomadura*.[11] It is unclear whether hydrogenation of the double bond in specific isoprene units changes the reactivity of the quinone system. The double bonds present within the isoprenyl side chain are not conjugated to the quinone system within MK. Therefore, it would not be anticipated that a significant change in the quinone redox potential would occur upon reduction of an isoprenyl unit. However, it has been reported that even when there is no direct conjugation between the quinone system and a substituent group, electrochemical reduction of the quinone system is sensitive to the electronic perturbation of the substituents.[1] Thus, it is possible that partial saturation in the isoprenyl side chain could influence the quinone redox potential, where an indirect through-bond effect could be a contributing factor and/or conformational effects of the substituent. Therefore, we hypothesized that the quinone redox potential of MK-1 may

DOI: 10.1021/acs.biochem.9b00007
Biochemistry 2019, 58, 1596−1615

be influenced by the degree of saturation in the isoprenyl side chain.

In this work, MK-1 and MK-1(H_2) (Figure 1) were first synthesized and then their conformations within organic solvents were elucidated by one-dimensional (1D) and two-dimensional (2D) ^{1}H nuclear magnetic resonance (NMR) spectroscopy. MK-1 and MK-1(H_2) adopted similar folded−extended conformations in each solvent, but the preferred folded−extended conformations differed slightly between solvent environments. The quinone redox potentials of MK and MK-1(H_2) were measured in three organic solvents, where a solvent effect (presumably due to a change in the dielectric constant) was observed, and most interestingly, an ∼20 mV difference in semiquinone redox potential was observed between MK-1 and MK-1(H_2). The interaction of MK-1 and MK-1(H_2) with phospholipid monolayers was characterized using Langmuir phospholipid monolayers, and the two MK-1 analogues were found to interact with the phospholipid interface. Finally, using a complementary study, the location, orientation, and conformation of MK-1 and MK-1(H_2) within a reverse micelle (RM) model membrane interface were determined using 1D and 2D NMR spectroscopy. The two MK-1 analogues interacted similarly with the RM model membrane interface, and MK-1 adopted a slightly different folded conformation within the RM interface compared to that observed in an organic solution.

EXPERIMENTAL SECTION

Materials. Menadione (crystalline), sodium hydrosulfite (85.0%), 1,4-dioxane (99.9%), 3-methyl-2-buten-1-ol (99%), BF_3 etherate (≥46.5%), Luperox A98 benzoyl peroxide (≥98%), 1-iodo-3-methylbutane (97%), dioctyl sulfosuccinate sodium salt (AOT, 97.0%), isooctane (2,2,4-trimethylpentane, ≥99.0%), chloroform (99.8%), methanol (99.9%), tetrabutylammonium perchlorate (TBAP, ≥99.0%), ferrocene (Fc, anhydrous), silver nitrate ($AgNO_3$, ≥99.0%), and activated charcoal were purchased from Sigma-Aldrich and used as received unless otherwise noted. Absolute ethanol and ultra-high-purity argon gas (99.9%) were acquired from Pharmco-Aaper and Airgas, respectively. Deuterated solvents of acetonitrile (d_3-ACN or CD_3CN) (99.8% D), dimethyl sulfoxide (d_6-DMSO) (99.9% D, 0.05% (v/v) tetramethylsilane), and d_6-benzene (≥99.6%) were acquired from Sigma-Aldrich. Deuterium oxide (D_2O, 99.9%), d_2-dichloromethane (99.9%), and d_4-methanol (99.8%) were acquired from Cambridge Isotope Laboratories, Inc. Deuterated pyridine (99.8% D) was purchased from Arcos Organics. DPPC (1,2-dipalmitoyl-*sn*-glycero-3-phosphocholine, ≥99.0%) and DPPE (1,2-dipalmitoyl-*sn*-glycero-3-phosphoethanolamine, ≥99.0%) were purchased from Avanti Polar Lipids Inc. Monosodium phosphate (NaH_2PO_4, 96.0%) and sodium phosphate dibasic anhydrous (Na_2HPO_4) were purchased from Fisher Scientific, and distilled deionized water (DDI H_2O) was purified with a Barnstead E-pure system (∼18 MΩ cm).

General Methods. All non-aqueous reactions were carried out under an argon atmosphere in flame-dried glassware, and all mixtures were stirred on a magnetic stir plate using an anhydrous solvent unless otherwise noted. Reactions were monitored by thin layer chromatography (TLC) on Whatman Partisil K6F TLC plates (silica gel 60 Å, 0.250 mm thickness) and visualized using an ultraviolet lamp (366 or 254 nm). Products were purified by flash chromatography (SiliCycleSiliaFlash F60, 43−60 μm, 60 Å). Yields refer to chromatographically and spectroscopically (^{1}H NMR) homogeneous materials unless otherwise noted. All chemicals were used without purification except AOT and the organic solvents. AOT was purified using activated charcoal and methanol to remove acidic impurities using previously reported methods.[38] Organic solvents dimethyl sulfoxide (DMSO), acetonitrile (CH_3CN or ACN), and pyridine were purified by distillation and then dried over activated 3 Å molecular sieves (40 g/200 mL of solvent) for 3 days. Benzene was dried by being passed through an alumina drying column (Solv-Tek Inc.) under argon pressure. When samples were prepared for RM NMR experiments, deuterium oxide was used instead of H_2O and the pH was adjusted to consider the presence of deuterium (pD = 0.4 + pH).[39] ^{1}H and ^{13}C NMR spectra were recorded on a 400 MHz Varian Model MR400, 400 MHz Varian iNova400, or 500 MHz Varian iNova500 spectrometer. Chemical shift values (δ) are reported in parts per million and referenced against the internal solvent peaks in ^{1}H NMR ($CDCl_3$, δ 7.26; d_3-acetonitrile, δ 1.94; d_6-DMSO, δ 2.50; d_4-methanol, δ 4.87; d_2-methylene chloride, δ 5.32; d_6-benzene, δ 7.16; d_5-pyridine, δ 8.74; D_2O, δ 4.79) and in ^{13}C NMR ($CDCl_3$, δ 77.16; d_6-benzene, δ 128.06).

Preparation of 2-Methyl-3-(3-methylbut-2-en-1-yl)-naphthalene-1,4-dione, MK-1 (3). Menadiol **2** was synthesized as previously described[37] from menadione **4**, and MK-1 **3** was synthesized previously.[8] However, in this work, the reaction to form MK-1 **3** was scaled up and characterization reported data in $CDCl_3$. To a dry 100 mL Schlenk flask were added a stir bar, EtOAc (16 mL), and 1,4-dioxane (16 mL), which was then purged/evacuated with argon repeatedly. Then, crude menadiol **2** (2.50 g, 4:1 menadiol:menadione by NMR integration; note that menadiol is prone to autoxidation in $CDCl_3$, 11.48 mmol) was added followed by 3-methyl-2-buten-1-ol **1** (1.08 g, 12.52 mmol) and then dropwise addition of distilled BF_3 etherate (0.8 mL). The reaction solution turned dark orange and was refluxed at 70 °C for 3 h under argon. The reaction was quenched with ice and H_2O (100 mL), and then the mixture extracted with diethyl ether (3 × 100 mL). The yellow organic extracts were washed with saturated $NaHCO_3$ (100 mL), washed with brine (100 mL), dried with anhydrous Na_2SO_4, and then concentrated under reduced pressure at ambient temperature to yield 3.50 g of crude red oil. The crude oil was purified by flash column chromatography (1000 mL of 230−400 mesh SiO_2, 70 mm column, 20:1 *n*-pentane:EtOAc). The red oil obtained was dried under reduced pressure (∼125 mTorr) overnight to yield 0.628 g of a deep red oil (2.61 mmol, 22.7% yield): ^{1}H NMR (400 MHz, $CDCl_3$) δ 8.06−8.08 (m, 2H), 7.67−7.69 (m, 2H), 5.02 (t, J = 7.0 Hz, 1H), 3.36 (d, 2H, J = 7.0 Hz), 2.19 (s, 3H), 1.79 (s, 3H), 1.69 (s, 3H); ^{13}C NMR (101 MHz, $CDCl_3$) δ 185.6, 184.7, 146.2, 143.4, 134.1, 133.47, 133.42, 132.33, 132.30, 126.4, 126.3, 119.3, 26.3, 25.9, 18.2, 12.8; HRMS (DART) m/z [(M + H)$^+$] calcd for $C_{16}H_{17}O_2$ 241.1223, found 241.1222.

Preparation of 2-Isopentyl-3-methylnaphthalene-1,4-dione, MK-1(H_2) (6). To a dry 100 mL round-bottom Schlenk flask were added a stir bar and dry and degassed benzene (30 mL) followed by 1-iodo-3-methylbutane **5** (1.98 g, 10.0 mmol, 1 equiv), which was then purged/evacuated with argon repeatedly. To a dry 20 mL vial was added dry benzene (15 mL), which was then degassed via argon needle purge, followed by addition of menadione **4** (1.72 g, 10.0 mmol) and benzoyl peroxide (2.42 g, 10.0 mmol, 1 equiv). This solution

DOI: 10.1021/acs.biochem.9b00007
Biochemistry 2019, 58, 1596−1615

was sonicated until dissolution occurred under argon. The naphthoquinone/benzoyl peroxide solution was added dropwise over 135 min to the refluxing prenyl iodide solution, which was under an argon atmosphere during the reaction. After the addition was complete, the solution was refluxed for an additional 1 h. The solution was then diluted with saturated $NaHCO_3$ (100 mL) and diethyl ether (100 mL), and then the two phases were separated. The aqueous layer was extracted with diethyl ether (3 × 100 mL), and the combined organic extracts were washed with saturated $NaHCO_3$ (100 mL), washed with brine (100 mL), dried with anhydrous Na_2SO_4, and then concentrated under reduced pressure at ambient temperature to yield a crude yellow powder. The crude powder was purified by flash column chromatography (10:1.5 *n*-pentane:EtOAc) to yield 0.493 g of a yellow solid (2.03 mmol, 20.3% yield) after drying overnight under reduced pressure (~125 mTorr): ^{1}H NMR (400 MHz, C_6D_6) δ 8.05−8.07 (m, 2H), 7.04−7.06 (m, 2H), 2.41−2.45 (m, 2H), 1.92 (s, 3H), 1.45−1.55 (m, 1H), 1.16−1.21 (m, 2H), 0.89 (d, J = 6.6 Hz, 2H); ^{13}C NMR (101 MHz, C_6D_6) δ 184.9, 184.3, 147.5, 142.7, 133.09, 133.08, 132.74, 132.71, 126.26, 126.21, 37.8, 28.9, 25.2, 22.5, 12.3; HRMS (DART) m/z [(M + H)$^+$] calcd for $C_{16}H_{19}O_2$ 243.1380, found 243.1378.

Mass Spectrometry. High-resolution mass spectrometry (HRMS) experiments were conducted on an Agilent 6224 TOF LC/MS instrument [O-time-of-flight (TOF)] interfaced with the Direct Analysis in Real Time (DART) source (IonSense DART-100). A standard of Jeffamine was used as an internal standard calibration for HRMS DART experiments carried out in positive mode.

NMR Spectroscopic Studies. 1D and 2D ^{1}H NMR spectroscopic studies were carried out both in organic solvents and in an RM model membrane system. ^{1}H and ^{13}C NMR spectra were recorded using either a Varian model MR400, model Inova400, or model Inova500 spectrometer operating at either 400, 500, or 101 MHz, respectively. Chemical shift values (δ) are reported in parts per million and referenced against the internal solvent peaks in ^{1}H NMR ($CDCl_3$, δ 7.26; d_3-ACN, δ 1.94; d_6-DMSO, δ 2.50; d_4-methanol, δ 4.87; d_2-methylene chloride, δ 5.32; d_6-benzene, δ 7.16; d_5-pyridine, δ 8.74; D_2O, δ 4.79) and in ^{13}C NMR ($CDCl_3$, δ 77.16; d_6-benzene, δ 128.06). All NMR spectra were recorded at either 22, 25, or 26 °C. See figure captions and the Supporting Information for more details.

Solution 1D ^{1}H NMR Spectroscopic Studies. Samples were prepared by dissolving ~5.0 mg of MK-1 in 0.5 mL of either d_1-chloroform, d_2-methylene chloride, d_4-methanol, d_6-DMSO, d_5-pyridine, d_3-ACN, or d_6-benzene. The NMR instrument was locked onto the respective deuterium signal in the deuterated solvent used. NMR spectra were then collected using 32 scans for each sample. The data were processed using MestReNova NMR processing software version 10.0.1. The spectra were manually phased, and then the baseline was corrected using a Bernstein Polynomial Fit (polynomial order 3). The obtained spectra were referenced to the proper internal solvent peak.

Sample Preparation for ^{1}H−^{1}H 2D NOESY and ^{1}H−^{1}H 2D ROESY NMR Spectroscopic Studies. To prepare the solutions of MK-1 or MK-1(H_2) in d_5-pyridine, d_3-ACN, and d_6-DMSO, 0.0024 g of MK-1 or 0.0024 g of MK-1(H_2) was dissolved in 0.5 mL of a deuterated solvent to produce a 20 mM solution of MK-1 or MK-1(H_2), respectively. The NMR samples containing the MK-1 or MK-1(H_2) solution were purged with argon briefly and capped prior to data collection.

^{1}H−^{1}H 2D NOESY and ^{1}H−^{1}H 2D ROESY NMR Spectroscopic Solution Studies. ^{1}H−^{1}H 2D NOESY NMR and ^{1}H−^{1}H 2D ROESY NMR spectroscopic experiments were conducted using a 400 MHz Varian MR400 NMR spectrometer operating at 26 °C. A standard NOESY pulse sequence was used consisting of 256 transients with 16 scans in the f1 domain using a 500 ms mixing time, a 45° pulse angle, and a 1.5 s relaxation delay. The standard ROESYAD pulse sequence consisted of 256 transients with 16 scans in the f1 domain using a 400 ms mixing time, a 45° pulse angle, and a 2.0 s relaxation delay. The NMR was locked onto either d_5-pyridine, d_3-ACN, or d_6-DMSO. The resulting spectrum was processed using MestReNova NMR software version 10.0.1 (see the Supporting Information for further details). The spectra were referenced to the proper internal solvent peak.

Molecular Mechanics Calculations. To illustrate conformations for MK-1 and MK-1(H_2), Merck Molecular Force Field 94 (MMFF94) molecular mechanics gas phase simulations were conducted using ChemBio3D Ultra 12.0 at 25 °C. Starting conformations were obtained by building ChemDraw structures and rotating desired bonds, and then simulations were run followed by energy optimization or simply an energy minimization to achieve the desired conformation. Conformations A, A1, B, B1, C, and C1 in Figure 5 were constructed and then energy minimized with a root-mean-square (RMS) gradient of 0.1 and up to 50 iterations to obtain MK-1 and MK-1(H_2) conformations that agreed with our interpretation of the cross peak observations and intensities in the ^{1}H−^{1}H 2D NOESY and ROESY NMR spectral data. Two simulations were run for 10000 iterations and then energy minimized using an MMFF94 energy minimization calculation using 500 iterations with an RMS gradient of 0.001 to achieve conformations D and D1 in Figure S27. Conformations E, E1, F, and F1 in Figure S27 were generated by rotating bonds to achieve the desired conformation followed by an energy minimization using 20−50 iterations and an RMS gradient of 0.1. A table of structural parameters such as selected distances between hydrogens within the conformations in Figure 5 and Figure S27 and energies calculated for the three-dimensional (3D) conformations can be found in the Supporting Information. Tables of Cartesian coordinates for the MK-1 analogue conformations can be found in the Supporting Information.

Electrochemistry Methods. The electrochemistry was performed on a CHI 750D potentiostat. For cyclic voltammetry, a classical three-electrode system was used with a scan rate of 100 mV/s at ambient temperature. A glassy carbon working electrode (BASi MF2012, 3 mm) was lightly polished between runs with alumina powder and then rinsed with water and ethanol. A platinum wire counter electrode (BASi MW1032) was gently polished between runs with 600 grit sandpaper. A Ag^+/Ag reference electrode (BASi MW1085) was constructed by using the Ag wire gently polished with 600 grit sandpaper inserted into a freshly prepared solution of organic solvent (ACN, pyridine, or DMSO) with 0.1 M TBAP and 0.01 M $AgNO_3$. This reference electrode was equilibrated in the MK-1 or MK-1(H_2) solution (2 mM) of the same organic solvent for 10 min. The solutions were bubbled for ~5−10 min with argon gas to ensure as much dissolved O_2(g) was removed as possible before the cyclic voltammogram was recorded. All half-wave potentials recorded were referenced to

DOI: 10.1021/acs.biochem.9b00007
Biochemistry 2019, 58, 1596−1615

the internal standard Fc^+/Fc couple by subtracting the averaged potential in each solvent. The Fc^+/Fc couple against the Ag^+/Ag reference in ACN was 0.081 ± 0.002 V, in DMSO was 0.176 ± 0.004 V, and in pyridine was 0.562 ± 0.001 V. The reliability of the Fc^+/Fc couple half-wave potential in each solvent was within experimental error.

$$E_{1/2} = \frac{E_{pc} + E_{pa}}{2} \quad (1)$$

$$\frac{i_{pc}}{i_{pa}} = 1, \text{ for a reversible process} \quad (2)$$

$$\Delta E_p = E_{pc} - E_{pa},\ n = x \times \frac{0.059V}{\Delta E_p} \quad (3)$$

The half-wave potentials are calculated using eq 1, where E_{pc} and E_{pa} are the cathodic and anodic peak potentials, respectively. The cathodic and anodic peak currents, i_{pc} and i_{pa}, respectively, were measured manually with a ruler on the cyclic voltammograms in centimeters to determine reversibility as a measure of the closeness to unity (eq 2). The number of electrons, n, in each process was determined using eq 3, where x is the adjustment factor in each solvent determined by setting the standard ferrocene number of electrons to 1 (n = 1). Electrochemistry performed in non-aqueous solvents may have ΔE_p values that are not indicative of the number of electrons; therefore, the ferrocene standard was used to determine the true value. See the Supporting Information for more detailed electrochemistry methods and discussion.

Langmuir Monolayer Compression Isotherms. Langmuir phospholipid monolayers were prepared using a Kibron μtroughXS. The subphase consisted of ∼50 mL of a 20 mM phosphate buffer (pH 7.4). Phospholipid stock solutions of 18.4 mg (1 mM) of DPPC or 17.3 mg (1 mM) of DPPE were prepared by dissolving the phospholipid in 25 mL of a chloroform/methanol solvent [9:1 (v/v)]. Stock solutions (1 mM) of both MK-1 and MK-1(H_2) were prepared with 0.97 and 0.96 mg, respectively, in 4 mL of a chloroform/methanol solvent [9:1 (v/v)]. Then, 20 μL of a stock solution [20 nmol of DPPC, DPPE, MK-1, or MK-1(H_2)] or a mixture (10 nmol of lipid and 10 nmol of MK) was applied in dropwise fashion to the surface of the subphase. This was then allowed to equilibrate for 15 min, allowing the lipids to spread and the solvent to evaporate. The DPPC/DPPE mixed solution and MK-1 or MK-1(H_2) were prepared by mixing equimolar amounts of phospholipid and MK analogue in a separate vial before application to the subphase. The resulting monolayer was compressed at a rate of 10 mm min^{-1} (5 mm min^{-1} from two sides) with a Teflon ribbon, and the surface tension was measured using the Wilhemy plate method using a wire probe as the Wilhemy plate. The temperature of the compression isotherm experiments was kept consistent at 25 °C using a circulating water bath. The surface pressure reported is calculated from eq 4, where π is the surface pressure, γ_o is the surface tension of water without lipid (72.8 mN/m[40,41]), and γ is the surface tension of water with lipid present during compression. Each compression isotherm presented herein is an average of three measurements. The data acquired were processed using OriginPro version 9.1 graphing software. The compression modulus was calculated as described in the Supporting Information.

$$\pi = \gamma_o - \gamma \quad (4)$$

Sample Preparation for RM NMR Spectroscopic Studies. A 0.50 M AOT stock solution was prepared by dissolving AOT (5.56 g, 12.5 mmol) in isooctane (25.0 mL). Empty RMs were prepared by mixing a 0.50 M AOT stock solution with a D_2O water pool and then vortexed. MK-1 and MK-1(H_2) RMs were made in a similar manner, the only difference being a 14.3 mM stock solution for MK-1 or MK-1(H_2) was prepared by dissolving MK-1 or MK-1(H_2), respectively, in a 0.50 M AOT/isooctane solution. The RMs were then prepared using the MK-1 or MK-1(H_2) AOT/isooctane stock solution. First, 2.0 mL samples were made using specific amounts of MK-1 or MK-1(H_2) AOT/isooctane stock solution and then diluting the sample to 2.0 mL with the 0.50 M AOT/isooctane solution. From the 2.0 mL solutions, 1.0 mL RM samples were prepared using designated amounts of the 2.0 mL sample and then adding the proper amount of D_2O at pH 6.65 (see General Methods for pH measurements) for MK-1 [the D_2O pH was 6.71 for the MK-1(H_2) samples] to form RMs of the desired size. The samples were then vortexed until the solution was clear. The overall concentrations for the 1.0 mL MK-1 RM samples are as follows: w_0 4, 13.8 mM; w_0 8, 6.5 mM; w_0 12, 3.5 mM; w_0 16, 1.9 mM; and w_0 20, 1.3 mM. The overall concentrations for the 1.0 mL MK-1(H_2) RM samples are as follows: w_0 4, 13.8 mM; w_0 8, 6.4 mM; w_0 12, 3.5 mM; w_0 16, 2.0 mM; and w_0 20, 1.4 mM.

1D ^{1}H NMR Spectroscopic Studies of AOT/Isooctane RMs Containing MK-1 or MK-1(H_2). NMR spectra of MK-1 and MK-1(H_2) in various size RMs, isooctane, and D_2O were obtained using a Varian Inova 400 MHz instrument operating at 22 °C using routine parameters (45° pulse angle and 1 s relaxation delay) and 64 scans. The NMR instrument was locked onto the 10% D_2O signal for the RM samples and locked onto 100% D_2O for the sample in D_2O. The 1D ^{1}H NMR spectra of MK-1 or MK-1(H_2) in isooctane were doped with ∼5% d_6-benzene for the NMR instrument to lock onto and to achieve properly shimmed spectra. The spectral data were processed using MestReNova NMR processing software version 10.0.1. The spectra were manually phased, and then the baseline was corrected using a multipoint baseline correction (cubic splines). The spectrum in D_2O was referenced to the internal D_2O peak, and the spectra in isooctane and RMs were referenced to the isooctane methyl peak (0.904 ppm) as previously reported.[39]

Sample Preparation for ^{1}H−^{1}H 2D NOESY and ^{1}H−^{1}H 2D ROESY NMR Spectroscopic Studies in AOT/Isooctane RMs. RM samples of MK-1 and MK-1(H_2) were prepared in the following manner. A 0.50 M AOT stock solution was first prepared by dissolving AOT (5.56 g, 12.5 mmol) in isooctane (25.0 mL). A 1.0 mL stock solution of 112 mM MK-1 in an AOT/isooctane solution was prepared by dissolving 27.7 mg of MK-1 in 1.0 mL of a 0.50 M AOT/isooctane stock solution. To prepare a w_0 12 RM, 894.68 μL of a 112 mM MK-1 AOT/isooctane stock solution and 105.32 μL of D_2O at pH 7.03 were mixed together and then vortexed until the solution was clear. The MK-1(H_2) w_0 12 RM sample was prepared like that of MK-1 using a 112 mM stock solution and D_2O (pH 7.01). This final mixture results in a w_0 12 RM microemulsion with an overall concentration of MK-1 or MK-1(H_2) of ∼100 mM (∼29 molecules per RM). The NMR samples containing the MK-1 or MK-1(H_2) RM solution were purged with argon briefly and capped prior to data collection.

^{1}H−^{1}H 2D NOESY and ^{1}H−^{1}H 2D ROESY NMR Spectroscopic Studies in a w_0 12 AOT/Isooctane RM.

DOI: 10.1021/acs.biochem.9b00007
Biochemistry 2019, 58, 1596−1615

Scheme 1. (A) Synthetic Scheme for the Allylic Alcohol Coupling Reaction To Form MK-1 3 and (B) Synthetic Scheme for the Radical Alkylation of Menadione 4 and 1-Iodo-3-methylbutane 5 To Form MK-1(H_2) 6[8,37,51−53]

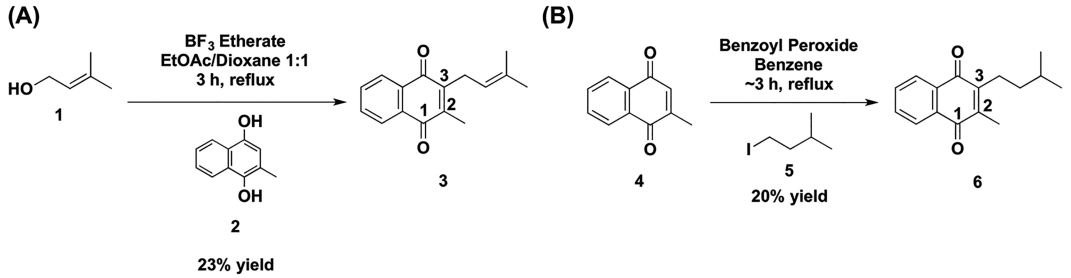

2D NMR spectra of MK-1 and MK-1(H_2) in RMs were obtained using similar conditions and methods described previously[37,42,43] using a 400 MHz Varian MR400 NMR spectrometer operating at 26 °C for MK-1 and were obtained using a 500 MHz Varian Inova 500 spectrometer operating at 25 °C for MK-1(H_2). A standard NOESY pulse sequence was used consisting of 200 or 256 transients with either 16 or 32 scans in the f1 domain using a 200 ms mixing time, a 45° pulse angle, and a 1.5 s relaxation delay. A standard ROESYAD pulse sequence was used consisting of 256 transients with 16 scans in the f1 domain using a 200 ms mixing time, a 45° pulse angle, and a 2.0 s relaxation delay. The NMR instrument was locked onto the 10% D_2O signal. The resulting spectrum was processed using MestReNova NMR software version 10.0.1 (see the Supporting Information for further details). The spectrum was referenced to the isooctane methyl peak at 0.904 ppm on both axes as previously reported.[39] The 3D conformation illustration within an RM interface was constructed using ChemDraw Professional 15.0 and Chem-Bio3D Ultra 12.0 based on spectral parameters described in Results and Discussion.

Dynamic Light Scattering (DLS) Studies. RMs for DLS studies were prepared as described for the NMR spectroscopic studies except that DDI H_2O was used as the water pool instead of D_2O and 0.50 M AOT was diluted with isooctane after the RM had formed to a final AOT concentration of 0.1 M. The hydrodynamic radius of the RMs was determined by DLS measurements performed on a Malvern Zetasizer Nano ZS instrument (Malvern Instruments, Malvern, U.K.). The DLS cuvette (1 cm × 1 cm, glass) was washed three times with isooctane followed by three washes with the RM sample. Then, the cuvette was filled with 1 mL of the RM sample and closed with a Teflon cap. Each experiment was conducted at 25 °C and consisted of a 700 s sample equilibration period followed by 10 measurements consisting of 15 scans each.[42] Each sample was measured in triplicate, and the radius and polydispersity (PDI) were recorded. The data were analyzed using Malvern Zetasizer Software version 7.11 and compared to values reported in the literature.[44] See the Supporting Information for data and interpretation.

RESULTS AND DISCUSSION

Synthesis and Characterization of MK-1 Analogues. We have previously synthesized MK-1,[8] and it has been synthesized by other reported routes;[45−49] however, here we present a scaled-up version and NMR spectral characterization in chloroform-*d* (Scheme 1). Menadiol **2** was synthesized as previously described from menadione **4**.[37,50,51] To introduce the isoprenyl side chain, menadiol **2** was treated with 3-methyl-2-buten-1-ol **1** in the presence of the Lewis acid catalyst, boron trifluoride.[37,51] MK-1 **3** was obtained as a red oil in a 23% yield (Scheme 1). Although the route to obtain MK-1(H_2) has been reported in the literature[52] (Scheme 1), the product was not isolated in pure form or characterized by NMR spectroscopy. We modified and optimized the reported route to increase the yield and scaled the reaction up to a preparatory scale using a similar methodology we recently reported.[53] MK-1(H_2) **6** was synthesized by a one-step radical alkylation reaction in which menadione **4** and 1-iodo-3,7-dimethylbutane **5** were coupled using benzoyl peroxide as the radical initiator.[52,53] MK-1(H_2) **6** was obtained as a yellow powder in a 20% yield (Scheme 1). The menadione/benzoyl peroxide solution was added dropwise over ∼2 h to the refluxing prenyl iodide solution to keep the stationary menadione **4** concentration sufficiently low in the reaction to ensure good selectivity of alkylation, favoring alkylation at C3 over C2 (Scheme 1).[52,53]

1D ^{1}H NMR Spectroscopic Studies of MK-1 in Organic Solvents. The synthesis of MK-1 and MK-1(H_2) provided material to investigate if the solvent environment induced chemical shift changes. NMR spectra of MK-1 were collected in various organic solvents ranging from aromatic to non-aromatic and of differing polarity (Figure 2). The most drastic chemical shift change observed for MK-1 was in the aromatic solvents, d_6-benzene and d_5-pyridine, compared to the other solvents in Figure 2. This is seen by focusing on the chemical

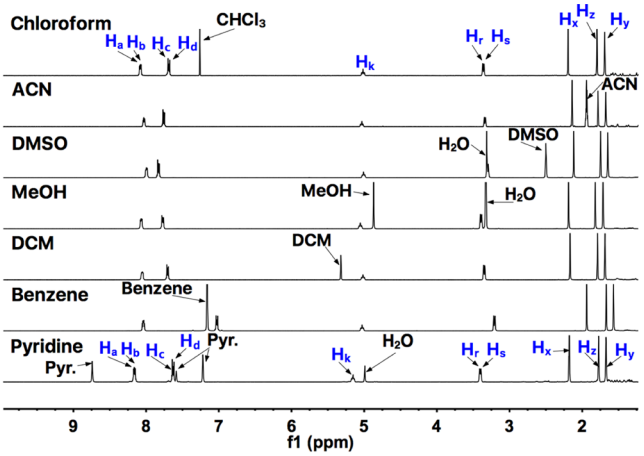

Figure 2. 1D ^{1}H NMR (400 MHz) spectra illustrating chemical shift differences of MK-1 hydrogens between various organic solvent environments. Abbreviations: ACN, d_3-acetonitrile; DMSO, d_6-dimethyl sulfoxide; MeOH, d_4-methanol; DCM, d_2-dichloromethane; Pyr, d_5-pyridine. A structure of MK-1 with a hydrogen labeling scheme key is shown in Figure 3.

DOI: 10.1021/acs.biochem.9b00007
Biochemistry 2019, 58, 1596−1615

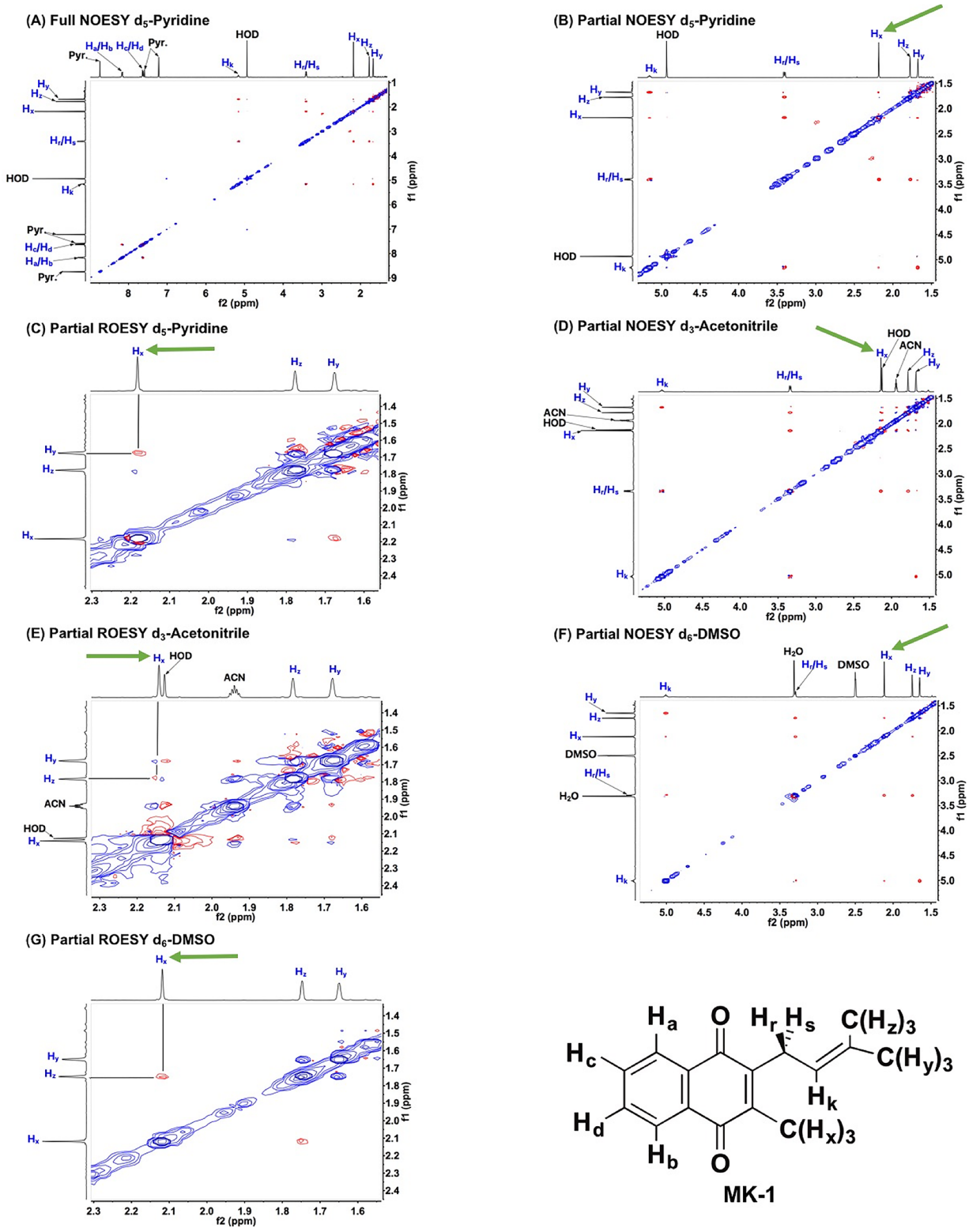

Figure 3. $^{1}H-^{1}H$ 2D NOESY and $^{1}H-^{1}H$ 2D ROESY NMR (400 MHz) spectra of 20 mM MK-1 in d_5-pyridine, d_3-acetonitrile (d_3-ACN), and d_6-DMSO at 26 °C. (A) Full $^{1}H-^{1}H$ 2D NOESY NMR spectrum of MK-1 in d_5-pyridine. (B) Partial $^{1}H-^{1}H$ 2D NOESY NMR spectrum of MK-1 in d_5-pyridine. (C) Partial $^{1}H-^{1}H$ 2D ROESY NMR spectrum of MK-1 in d_5-pyridine. (D) Partial $^{1}H-^{1}H$ 2D NOESY NMR spectrum of MK-1 in d_3-ACN. (E) Partial $^{1}H-^{1}H$ 2D ROESY NMR spectrum of MK-1 in d_3-ACN. (F) Partial $^{1}H-^{1}H$ 2D NOESY NMR spectrum of MK-1 in d_6-DMSO. (G) Partial $^{1}H-^{1}H$ 2D ROESY NMR spectrum of MK-1 in d_6-DMSO. Blue intensity contours represent negative NOEs or ROEs, and red intensity contours represent positive NOEs or ROEs. A standard NOESY pulse sequence consisting of 256 transients with 16 scans in the f1 domain using a 500 ms mixing time and a 1.5 s relaxation delay was used. A standard ROESYAD pulse sequence consisting of 256 transients with 16 scans in the f1 domain using a 400 ms mixing time and a 2.0 s relaxation delay was used. The structure of MK-1 is shown with a hydrogen labeling scheme key. Green arrows indicate hydrogen H_x, where the observed cross peaks differed the most between the three solvents studied.

DOI: 10.1021/acs.biochem.9b00007
Biochemistry 2019, 58, 1596−1615

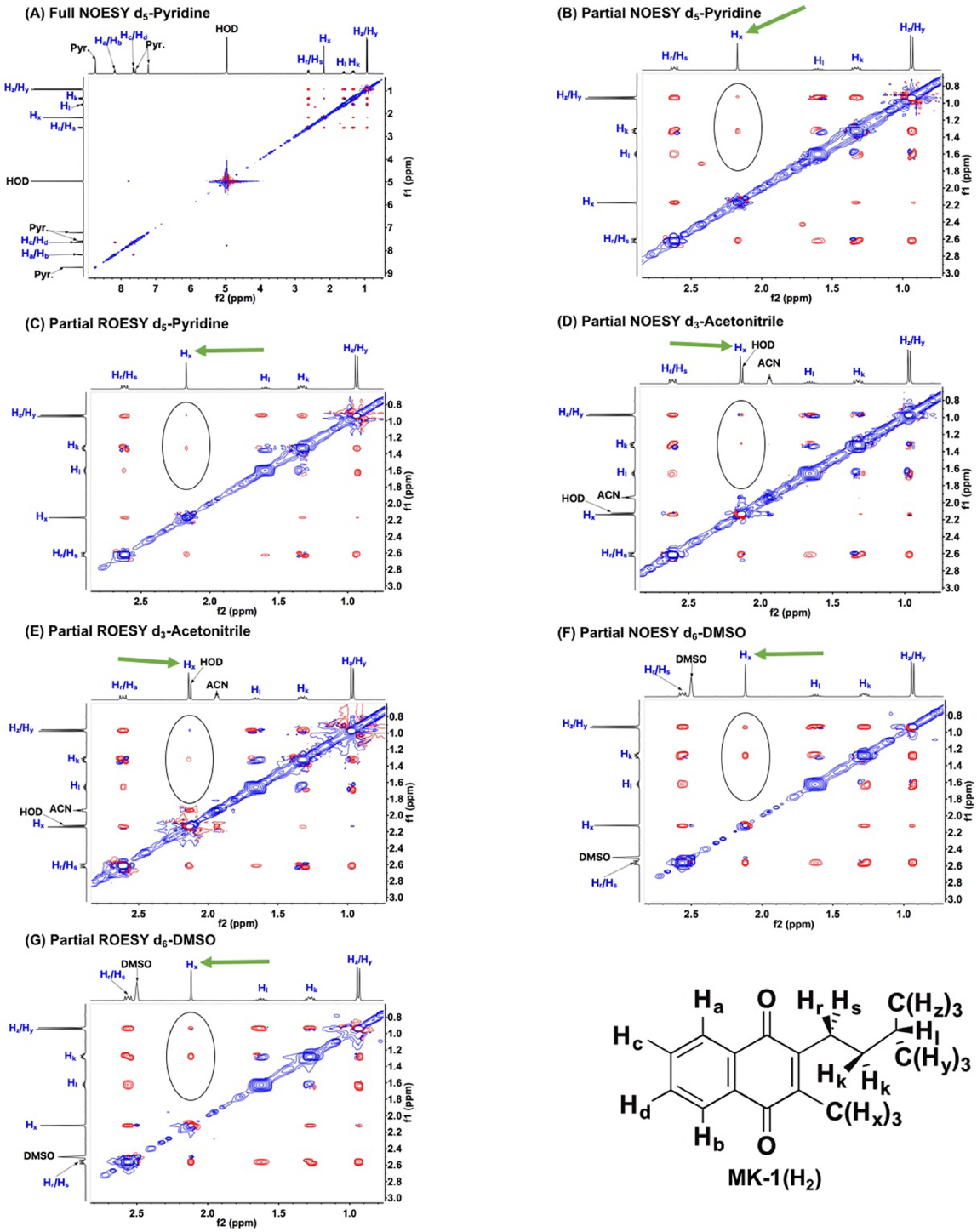

Figure 4. ^{1}H−^{1}H 2D NOESY and ^{1}H−^{1}H 2D ROESY NMR (400 MHz) spectra of 20 mM MK-1(H_2) in d_5-pyridine, d_3-acetonitrile (d_3-ACN), and d_6-DMSO at 26 °C. (A) Full ^{1}H−^{1}H 2D NOESY NMR spectrum of MK-1(H_2) in d_5-pyridine. (B) Partial ^{1}H−^{1}H 2D NOESY NMR spectrum of MK-1(H_2) in d_5-pyridine. (C) Partial ^{1}H−^{1}H 2D ROESY NMR spectrum of MK-1(H_2) in d_5-pyridine. (D) Partial ^{1}H−^{1}H 2D NOESY NMR spectrum of MK-1(H_2) in d_3-ACN. (E) Partial ^{1}H−^{1}H 2D ROESY NMR spectrum of MK-1(H_2) in d_3-ACN. (F) Partial ^{1}H−^{1}H 2D NOESY NMR spectrum of MK-1(H_2) in d_6-DMSO. (G) Partial ^{1}H−^{1}H 2D ROESY NMR spectrum of MK-1(H_2) in d_6-DMSO. Blue intensity contours represent negative NOEs or ROEs, and red intensity contours represent positive NOEs or ROEs. A standard NOESY pulse sequence consisting of 256 transients with 16 scans in the f1 domain using a 500 ms mixing time and a 1.5 s relaxation delay was used. A standard ROESYAD pulse sequence consisting of 256 transients with 16 scans in the f1 domain using a 400 ms mixing time and a 2.0 s relaxation delay was used. The structure of MK-1(H_2) is shown with a hydrogen labeling scheme key. Green arrows indicate hydrogen H_x, where the observed cross peaks differed the most between the two solvents studied, and black ovals highlight the region that changes the most between spectra.

shift differences observed between the MK-1 aromatic hydrogens, H_a/H_b and H_c/H_d. The chemical shift difference is nearly 1 ppm in d_6-benzene compared to 0.2−0.4 ppm in the other solvents. The methylene hydrogens, H_r/H_s, and the

DOI: 10.1021/acs.biochem.9b00007
Biochemistry 2019, 58, 1596−1615

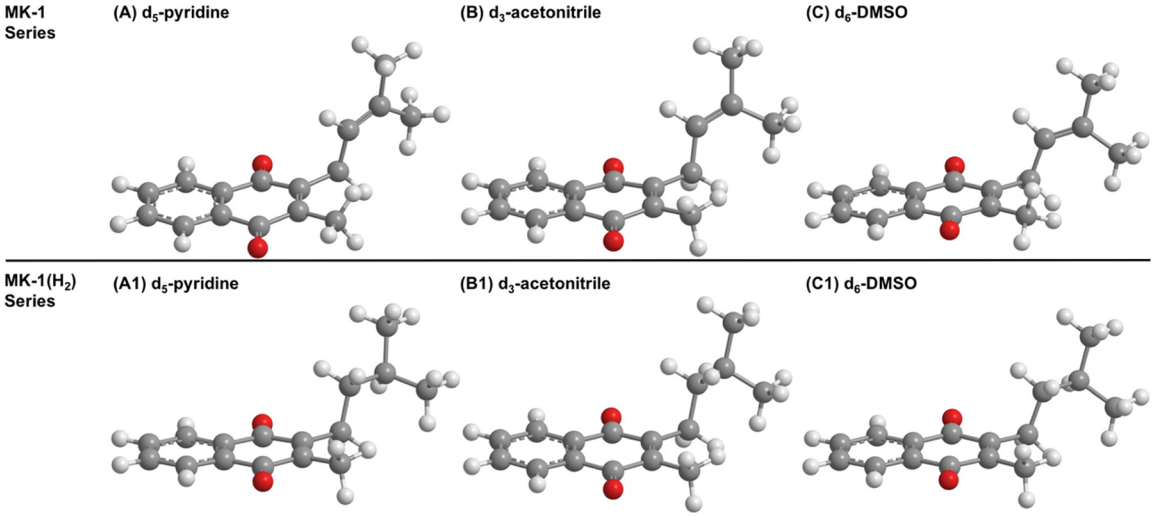

Figure 5. MK-1 and MK-1(H_2) conformations generated using MMFF94 calculations to illustrate the possible conformations consistent with the ^{1}H−^{1}H 2D NOESY and ROESY NMR spectral studies in which conformations agree with observed cross peak interactions and intensities. MK-1 series: (A) proposed MK-1 conformation in d_5-pyridine determined from ^{1}H−^{1}H 2D NOESY and ROESY NMR spectral data for cross peak interactions (51.8 kcal/mol; H_x−H_y, 4.3 Å), (B) proposed MK-1 conformation in d_3-ACN determined from ^{1}H−^{1}H 2D NOESY and ROESY NMR spectral data for cross peak interactions (48.6 kcal/mol; H_x−H_y, 3.9 Å), and (C) proposed MK-1 conformation in d_6-DMSO determined from ^{1}H−^{1}H 2D NOESY and ROESY NMR spectral data for cross peak interactions (47.3 kcal/mol; H_x−H_y, 3.2 Å). MK-1(H_2) series: (A1) proposed MK-1(H_2) conformation in d_5-pyridine determined from ^{1}H−^{1}H 2D NOESY and ROESY NMR spectral data for cross peak interactions (42.1 kcal/mol; H_x−H_z, 3.6 Å), (B1) proposed MK-1(H_2) conformation in d_3-ACN determined from ^{1}H−^{1}H 2D NOESY and ROESY NMR spectral data for cross peak interactions (43.0 kcal/mol; H_x−H_y, 4.0 Å), and (C1) proposed MK-1(H_2) conformation in d_6-DMSO determined from ^{1}H−^{1}H 2D NOESY and ROESY NMR spectral data for cross peak interactions (41.9 kcal/mol; H_x−H_y, 3.4 Å).

naphthoquinone methyl (H_x) also shift in d_6-benzene compared to the other solvents. Via examination of the chemical shift differences in the spectra in Figure 2, it is clear that MK-1 is influenced by solvent environment, but whether MK-1 adopts different conformations in these organic solvent environments remains unclear.

^{1}H−^{1}H 2D NOESY and ^{1}H−^{1}H 2D ROESY NMR Spectroscopic Studies of MK-1 and MK-1(H_2) in d_5-Pyridine, d_3-Acetonitrile, and d_6-DMSO. The 1D ^{1}H NMR experiments demonstrated that the solvent environment impacts the chemical environment surrounding MK-1 enough to change the observed chemical shift. However, whether the conformation of MK-1 and MK-1(H_2) changes depending on the solvent environment remained unclear. Therefore, we used two different complementary 2D NMR spectroscopic techniques (^{1}H−^{1}H 2D NOESY and ^{1}H−^{1}H 2D ROESY NMR) to elucidate the conformation of the MK analogues in organic solutions. We present the 2D NMR data for MK-1 in Figure 3, the 2D NMR data for MK-1(H_2) in Figure 4, and the 3D conformations for MK-1 and MK-1(H_2) in Figure 5. We used a semiquantitative approach for the 2D NMR conformational analysis in which NOE/ROE distance intensities are as follows: a strong cross peak intensity is an ∼2−3 Å distance, a medium cross peak intensity is an ∼3−4 Å distance, and a weak cross peak intensity is a >4 Å distance.[54] We standardized the signal intensities on the basis of the intensity of the H_a−H_c cross peak of MK-1 or MK-1(H_2), which was used as the internal intensity calibrant (the actual distance is 2.5 Å, which indicates a strong cross peak). Figure 3 shows ^{1}H−^{1}H 2D NOESY and ^{1}H−^{1}H 2D ROESY NMR spectra of MK-1 in d_5-pyridine, d_3-acetonitrile (d_3-ACN), and d_6-DMSO (see Figures S3−S11 and S16−S24 for full 2D NMR spectra and Figure S26 for ROE/NOE correlation traces). These organic solvents were chosen because they differed sufficiently with regard to shape, polarity, and aromatic versus non-aromatic and are well behaved in electrochemical studies.

The conformation of MK-1 in d_5-pyridine was determined by analyzing the ^{1}H−^{1}H 2D NOESY and ROESY NMR spectra (Figure 3A−C and Figures S3 and S4). Figure 3B shows a strong NOE cross peak observed between hydrogens $H_{r/s}$ and H_z and a weak NOE cross peak between $H_{r/s}$ and H_y (see the Supporting Information for hydrogen peak assignments of H_z and H_y). Weak NOE/ROE cross peaks are also observed between H_x and H_y (Figure 3B,C), which supports a folded−extended conformation in which the terminal methyl groups orient themselves in a manner to fold upward (C−C bond rotation allows the methyl groups to rotate upward) positioning H_y close enough to H_x to observe a NOE/ROE cross peak. The weak cross peak (same phase as the diagonal) observed between H_x and H_z is likely due to TOCSY exchange. The weak NOE cross peak in Figure 3B between H_x and H_k has an intensity similar to that of the NOE cross peak observed between H_x and H_y, which is not explained by an extended−flat conformation (see Figure S27E and Table S1 for structure and internuclear distances of the MK-1 flat−extended conformation). Together, these observations provide evidence that MK-1 adopts a folded-extended conformation in d_5-pyridine in which the isoprenyl side chain folds upward.

With regard to the conformation of MK-1 in d_3-ACN, panels D and E of Figure 3 (Figures S6 and S7) show a weak NOE/ROE cross peak observed between H_x and H_z and no cross peak observed between H_x and H_y. The cross peak observed is opposite in phase to the diagonal and possibly due to chemical exchange or TOCSY exchange. TOCSY exchange is more likely as are there are no readily exchangeable hydrogens in the molecule. There is a weak NOE cross peak between H_x and H_k that is visible only in the spectrum upon zooming in on lower floors, which is not consistent with an extended−flat

DOI: 10.1021/acs.biochem.9b00007
Biochemistry 2019, 58, 1596−1615

conformation and is different from that observed in d_5-pyridine, indicating slightly different conformations adopted between solvent environments. However, the cross peak intensity between $H_{r/s}$ and H_z or H_y is similar to that in d_5-pyridine. There is also a NOE/ROE cross peak observed between H_y and HOD and between H_y and the solvent, d_3-ACN, and interactions between MK and the solvent were not observed in the 2D NMR spectra of MK-1 in d_5-pyridine or d_6-DMSO. On the basis of observations described above, MK-1 likely adopts a folded−extended conformation in d_3-ACN that differs slightly from the folded−extended conformation in d_5-pyridine.

Finally, the conformation of MK-1 in d_6-DMSO was determined. Panels F and G of Figure 3 (Figures S9 and S10) show a weak NOE cross peak between H_x and H_k and a medium NOE/ROE cross peak between H_x and H_z and with no NOE/ROE cross peak observed between H_x and H_y. This is similar to the cross peaks observed in d_3-ACN, but the H_x to H_z cross peak is stronger in d_6-DMSO, indicating slightly different conformations. These observations would not be explained by a flat−extended conformation, and MK-1 likely adopts a folded−extended conformation in d_6-DMSO more similar to that in d_3-ACN than in d_5-pyridine.

To investigate whether saturation of the alkene in the isoprenyl side chain influences the conformation of MK-1(H_2), ^{1}H−^{1}H 2D NOESY and ^{1}H−^{1}H 2D ROESY NMR spectra were collected in d_5-pyridine, d_3-ACN, and d_6-DMSO (Figure 4). Similar NOE/ROE cross peaks were observed for MK-1(H_2) in d_5-pyridine and MK-1 in d_5-pyridine (Figure 4A−C and Figures S16 and S17). Specifically, a weak NOE/ROE cross peak between H_x and H_z/H_y, a medium NOE/ROE cross peak between H_x and $H_{r/s}$, and a medium NOE/ROE cross peak between $H_{r/s}$ and H_y were observed. There is also no NOE/ROE cross peak observed between H_x and H_l, which further supports a folded−extended conformation. This is suggestive of a similar conformation for MK-1(H_2) and MK-1 in d_5-pyridine, where both adopt a similar folded−extended conformation. Similar NOE/ROE cross peaks were observed for MK-1(H_2) in d_3-ACN and MK-1 in d_3-ACN (Figure 4D,E and Figures S19 and S20). Specifically, the lack of an observable cross peak between H_x and H_z/H_y (compared to a weak NOE/ROE cross peak in the case of MK-1), a medium NOE/ROE cross peak between H_x and $H_{r/s}$, a medium NOE/ROE cross peak between $H_{r/s}$ and H_y, and a very weak NOE/ROE cross peak between H_x and H_k was observed. There is also no NOE/ROE cross peak observed between H_x and H_l. This is suggestive of a similar conformation for MK-1(H_2) and MK-1 in d_3-ACN, where both adopt a similar folded−extended conformation. Comparable NOE/ROE cross peaks were observed for MK-1(H_2) in d_6-DMSO and MK-1 in d_6-DMSO (Figure 4F,G and Figures S22 and S23). For instance, a medium NOE/ROE cross peak between H_x and H_z/H_y, a medium NOE/ROE cross peak between H_x and $H_{r/s}$, a medium NOE/ROE cross peak between $H_{r/s}$ and H_y/H_z, and a medium NOE/ROE cross peak between H_x and H_k were observed. There was also no NOE/ROE cross peak observed between H_x and H_l. This is suggestive of a comparable conformation for MK-1(H_2) and MK-1 in d_6-DMSO, where both adopt a similar folded−extended conformation.

Considering the similar trends in cross peaks and intensities observed for MK-1 and MK-1(H_2) in d_5-pyridine, d_3-ACN, and d_6-DMSO, it appears that saturation does not affect the conformation significantly. The subtle differences observed for MK-1 and MK-1(H_2) in the different organic solvents suggest that slightly different folded−extended conformations are adopted between each of the organic solvents, but MK-1 and MK-1(H_2) have very similar conformations in each solvent. This suggests that there could be a correlation between a preferred conformation in each solvent environment and that a simple change such as saturation of a double bond only slightly influences this preferred conformation. Overall, these truncated MK analogues appear to adopt folded−extended conformations in organic solutions based on the 2D NMR data and the folded−extended conformations differ slightly between solvent environments. However, it is possible that an equilibrium population exists between multiple conformations (e.g., folded and/or nonfolded conformations). The observations from the 2D NMR spectroscopic studies support our first hypothesis that the most fundamental MK-1 analogues adopt folded conformations regardless of the degree of saturation in their isoprenyl side chain.

Illustrating MK-1 and MK-1(H_2) Conformations Using Molecular Mechanics. To clearly show illustrations of MK-1 and MK-1(H_2), conformations were generated on the basis of our interpretation of observed cross peak intensities in the ^{1}H−^{1}H 2D NOESY and ROESY NMR spectral data using a semiquantitative approach. We used molecular mechanics (MM) calculations to illustrate and model these conformations. This allowed us to explore the energy surface of conformations corresponding to MK-1 or MK-1(H_2) in either d_5-pyridine, d_3-ACN, or d_6-DMSO determined from the spectral data and provided a means for a visual comparison between conformations (Figure 5). Specific conformations were generated by constraining internuclear distances consistent with the observed 2D NMR spectral data and then energy optimized to calculate an energy value as well as produce realistic bond lengths and angles.

One of the low-energy conformations generated for MK-1 (Figure 5A; 51.8 kcal/mol; H_x−H_y, 4.3 Å) is consistent with the 2D NOESY/ROESY spectral parameters in d_5-pyridine. A lower-energy conformation for MK-1 (Figure 5B; 48.6 kcal/mol; H_x−H_z, 3.9 Å) is consistent with the 2D NOESY/ROESY spectral parameters in d_3-ACN. A slightly lower-energy conformation for MK-1 (Figure 5C; 47.3 kcal/mol; H_x−H_z, 3.2 Å) is consistent with the 2D NOESY/ROESY spectral parameters in d_6-DMSO. One of the low-energy conformations generated for MK-1(H_2) (Figure 5A1; 42.1 kcal/mol; H_x−H_z, 3.6 Å) is consistent with the NOESY/ROESY spectral parameters in d_5-pyridine. A conformation with a slightly higher energy for MK-1(H_2) (Figure 5B1; 43.0 kcal/mol; H_x−H_z, 4.0 Å) is consistent with the 2D NOESY/ROESY spectral parameters in d_3-ACN. A lower-energy conformation for MK-1(H_2) (Figure 5C1; 41.9 kcal/mol; H_x−H_z, 3.4 Å) is consistent with the 2D NOESY/ROESY spectral parameters in d_6-DMSO. All six of these conformations exhibit folding of the isoprenyl side chain upward out of the quinone plane (Figure 5) and can be described as folded−extended conformations. Each conformation for MK-1(H_2) is very similar to that of MK-1 in each organic solvent environment examined based on 2D NMR studies.

For comparison, conformations seen in panels D and D1 of Figure S27 are the lowest-energy conformations we found for MK-1 or MK-1(H_2), where an extended−flat conformation was subjected to a MM simulation using 10000 iterations followed by an energy minimization, which illustrates that folded conformations are easily reached and energetically

DOI: 10.1021/acs.biochem.9b00007
Biochemistry 2019, 58, 1596−1615

Scheme 2. Illustration of the One-Electron Reduction of the Quinone (Q) of MK-1 to the Semiquinone Radical Anion ($Q^{\bullet-}$) and the Second One-Electron Reduction to the Dianion (Q^{2-})

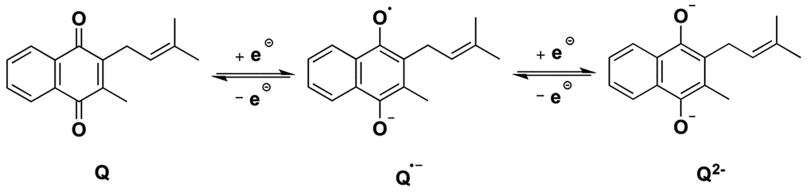

favorable. In addition to the folded conformations shown in Figure 5, a series of alternative flat conformations for MK-1 and MK-1(H_2) (panels E, E1, F, and F1 of Figure S27) were also generated on the basis of what is commonly seen in life science textbooks and literature and then subjected to energy optimization.[12,55,56] These flat−extended conformations are ∼11−20 kcal/mol higher than the lowest-energy conformations of MK-1 and MK-1(H_2). A table of selected internuclear distances for conformations seen in Figure 5 and Figure S27 is given in the Supporting Information.

Importantly, the folded−extended conformations for MK-1 determined in an organic solution closely resemble the folded conformation of the first isoprene unit of MK-2 (containing two isoprene units), which we determined previously in the same organic solvent environments.[37]

Reactivity of MK-1 and MK-1(H_2) in Different Organic Solvents: Electrochemistry. To determine the effect of saturation of the MK isoprenyl side chain on the quinone redox potential, we used cyclic voltammetry to measure the redox potentials of MK-1 and MK-1(H_2). Both MK-1 and MK-1(H_2) have two reversible single-electron redox processes; the first is the quinone to semiquinone ($Q/Q^{\bullet-}$) process, and the second the semiquinone to dianion ($Q^{\bullet-}/Q^{2-}$) process (Scheme 2). The half-wave potentials for each redox process $Q/Q^{\bullet-}$ and $Q^{\bullet-}/Q^{2-}$ in each solvent for MK-1 and MK-1(H_2) are listed in Table S9, and cyclic voltammograms are shown in Figure 6. The electrolyte tetrabutylammonium perchlorate (TBAP) was chosen because of its excellent solubility in all organic solvents. Furthermore, the addition of TBAP to MK-1 solutions in each solvent did not affect the observed chemical shifts of the MK-1 hydrogens, and thus, no evidence of ion pairing or association was found (see Figure S28). The water content of the solvents can affect the semiquinone $Q^{\bullet-}/Q^{2-}$ process as acidic hydrogens influence hydroquinone production, which results in potentials that approach the quinone $Q/Q^{\bullet-}$ half-wave potentials, and therefore, we compared only the first redox process, $Q/Q^{\bullet-}$, in our analyses.[57,58] Thus, it was important that we carried out our electrochemical experiments in anhydrous aprotic organic solvents as this issue is then avoided and organic solvents more closely resemble the native MK environment within a cellular membrane compared to aqueous solutions.

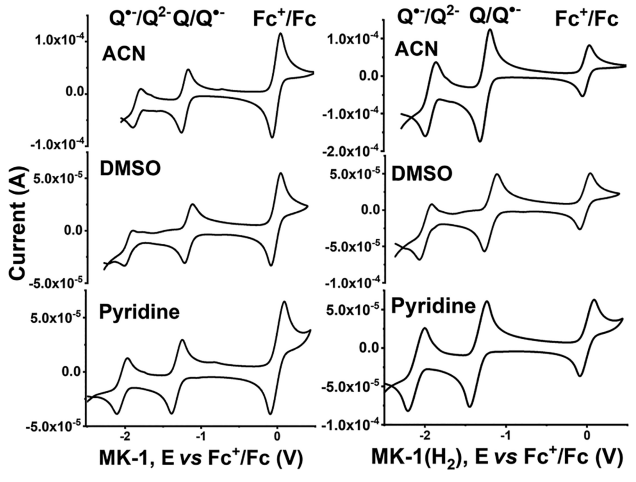

Figure 6. Six cyclic voltammograms of 2 mM MK-1 and MK-1(H_2) in ACN, DMSO, and pyridine. The potentials are referenced to the Fc^+/Fc couple internal standard (2 mM) determined in each solvent. From left to right, redox processes are $Q^{\bullet-}/Q^{2-}$, $Q/Q^{\bullet-}$, and Fc^+/Fc, respectively. Each sample has 0.1 M TBAP and was degassed with argon gas for 10 min at ambient temperature before spectra were recorded. Current sweeps are in the anodic direction from −2 to 1 V and back to −2 V vs Ag/AgCl. A 100 mV/s scan rate was used.

As shown in Figure 6, the ferrocene couple, Fc^+/Fc, was used as an internal reference standard so that the half-wave potentials are set to 0 V versus Fc^+/Fc. The values of $Q/Q^{\bullet-}$ $E_{1/2}$ versus Fc^+/Fc for MK-1 in ACN, DMSO, and pyridine were measured to be −1.227 ± 0.002, −1.158 ± 0.002, and −1.319 ± 0.001 V, respectively. The values of $Q/Q^{\bullet-}$ $E_{1/2}$ versus Fc^+/Fc for MK-1(H_2) in ACN, DMSO, and pyridine were measured to be −1.247 ± 0.007, −1.179 ± 0.002, and −1.343 ± 0.001 V, respectively. The values of $Q/Q^{\bullet-}$ $E_{1/2}$ versus Fc^+/Fc are near those reported for 1,4-naphthoquinone and those previously reported by our group for MK-2.[37,59,60] The values $Q^{\bullet-}/Q^{2-}$ $E_{1/2}$ versus Fc^+/Fc for MK-1 in ACN, DMSO, and pyridine were measured to be −1.882 ± 0.014, −1.949 ± 0.006, and −2.037 ± 0.005 V, respectively. The values of $Q^{\bullet-}/Q^{2-}$ $E_{1/2}$ versus Fc^+/Fc for MK-1(H_2) in ACN, DMSO, and pyridine were measured to be −1.912 ± 0.009, −1.9947 ± 0.0008, and −2.109 ± 0.005 V, respectively. The measured quinone half-wave redox potential differences in these solvents are statistically significant as they are distinctly different from each other at high confidence intervals (see Figure 7 caption and the Supporting Information).

The difference in millivolts between the unsaturated MK-1 and the saturated MK-1(H_2) quinone redox potential in each solvent of the less variable $Q/Q^{\bullet-}$ process is of the same magnitude as ∼20 mV with specific values of 20.033 ± 0.007, 21.333 ± 0.002, and 23.917 ± 0.001 mV for ACN, DMSO, and pyridine, respectively (Figure 7). The $Q/Q^{\bullet-}$ process potentials are less variable as the presence of acidic hydrogens and/or water can create the hydroquinone species, which results in the $Q^{\bullet-}/Q^{2-}$ process coalescing onto the first redox potential. Our previous work with MK-2 demonstrated that the isoprenyl side chain folds over toward the naphthoquinone moiety and that the solvent environment can influence the preferred conformation.[37] The mixing of molecular orbitals (MOs) on the naphthoquinone moiety with the isoprenyl side chain may potentially result in different energies of the electrochemical band gap (or HOMO to LUMO gap) needed

DOI: 10.1021/acs.biochem.9b00007
Biochemistry 2019, 58, 1596−1615

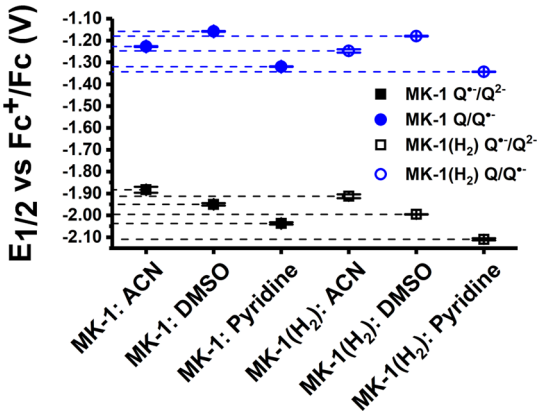

Figure 7. Measured $E_{1/2}$ (vs Fc^+/Fc in volts) of MK-1 and MK-1(H_2) $Q/Q^{\bullet-}$ and $Q^{\bullet-}/Q^{2-}$ redox process vs solvent. Each solvent was run in triplicate, with error bars shown. Added horizontal lines show the distinction between each solvent for each redox process. All solvent comparisons (ACN vs DMSO, etc.) for each redox process half-wave potential for MK-1 or MK-1(H_2) are statistically different with Student's *t* test confidence intervals of 99.9% ($p < 0.0001$), except for that of the ACN vs DMSO $Q/Q^{\bullet-}$ of MK-1, which was 99.5% ($p < 0.0016$) (four degrees of freedom). Comparisons between MK-1 and MK-1(H_2) half-wave potentials of $Q/Q^{\bullet-}$ and $Q^{\bullet-}/Q^{2-}$ for each solvent were at the 99.9% ($p < 0.0001$) confidence level, except for those of ACN, which were 98% ($p < 0.0089$) and 95% ($p < 0.0355$), respectively (four degrees of freedom). See the Supporting Information for data.

to reduce the quinone carbonyl oxygen to an anionic oxygen radical. The electrochemical band gap is suggestive of the potential observed or the energy required to reduce or oxidize an electrochemical process. This difference in the band gap energy results in unique half-wave potentials as the energy (E) and potential difference (V) are directly proportional as shown clearly by the electrostatic equation $E = VQ$, where Q is charge. The saturation or unsaturation of the isoprenyl side chain can therefore potentially influence these MOs and may alter the quinone redox potential in this manner. The semiquinone redox potential difference of ~20 mV between MK-1 and MK-1(H_2) could indicate the band gap energy difference between the saturated and unsaturated double bond in the one-unit isoprenyl side chain. However, the difference of ~20 mV is most likely due to an indirect effect manifested by a through-bond electronic change by the isoprenyl substituent on the quinone. An indirect substituent effect was used to explain a redox potential change for an N-aromatic substituent on a quinone.[1] The conformational differences in MK-1 between solvents were small, and the short isoprenyl side chain has limited spatial reach toward the naphthoquinone. If such an effect existed between conformation and redox potential, it may not be evident in the one-isoprene unit system. However, suitable high-level computational calculations should be carried out to characterize the HOMO−LUMO gap of this system and determine the exact contributions to the observed ~20 mV difference.

We also observed a trend in the data of the potential difference for the $Q/Q^{\bullet-}$ process as compared by solvent versus degree of saturation (Table S10). For MK-1 and MK-1(H_2), the potential differences in the $Q/Q^{\bullet-}$ process between ACN and DMSO are 69.250 ± 0.003 and 67.950 ± 0.008 mV, respectively. The other solvent comparisons also yield values that agree with each other. For MK-1 and MK-1(H_2), the potential differences in the $Q/Q^{\bullet-}$ process between DMSO and pyridine are 161.050 ± 0.002 and 163.633 ± 0.002 mV, respectively. Similarly, the potential differences of MK-1 and MK-1(H_2) of the $Q/Q^{\bullet-}$ process between ACN and pyridine are 91.800 ± 0.003 and 95.683 ± 0.008 mV, respectively. This conserved difference in the $Q/Q^{\bullet-}$ half-wave potentials between MK-1 and MK-1(H_2) in each solvent may signify that how the isoprenyl side chain folds is truly solvent-dependent and/or may suggest that the conformation of the short isoprenyl side chain (five carbons) of MK-1 has little effect on the observed quinone redox potential in the one-isoprene unit system.

In summary, both MK-1 and MK-1(H_2) during the first electrochemical process producing the semiquinone have the most positive potentials in DMSO and the most negative potentials in pyridine, demonstrating MK-1 or MK-1(H_2) is slightly more reducible in DMSO than in ACN or pyridine. Most remarkably, the observation of an ~20 mV change in quinone $Q/Q^{\bullet-}$ $E_{1/2}$ between MK-1 and MK-1(H_2) supports our second hypothesis that saturation of the isoprenyl side chain of MK-1 affects the observed quinone redox potential. This is the first time that these subtle changes have been demonstrated in a quinone/MK system. The difference is presumably mainly due to a through-bond indirect effect, which results in an electronic perturbation of the quinone system upon saturation of the isoprenyl side chain. There was not a large difference between the MK-1 analogue conformations, and therefore, changes in the observed redox potentials are not likely due to conformational differences. However, a potential correlation should be investigated using the appropriate fully unsaturated and partially saturated MK-2 analogues in combination with computational methods to determine if conformational folding of the second isoprene unit can alter the quinone redox potential in MK analogues with an unsaturated versus a partially saturated isoprenyl side chain.

Interaction of Langmuir Phospholipid Monolayers with MK-1 and MK-1(H_2). To understand the interaction and conformation of fundamental MK analogues within a membrane environment, we focused on characterizing the interaction of the most simple, truncated MK analogues, MK-1 and MK-1(H_2), with model membrane interfaces. Model membrane systems, such as Langmuir phospholipid monolayers, liposomes, micelles, and RM microemulsions, have been used to characterize the interaction and location of probe molecules with membranelike interfaces (Figure 8).[44,61−69] Langmuir phospholipid monolayers and RMs are two complementary model membrane systems that together can be used to characterize the interaction, location, placement, and conformation of MKs within a model membrane interface. Using these two model membrane systems together allowed us to determine whether MK-1 analogues interact with model membrane interfaces and if a folded conformation is adopted within the RM model membrane interface.

Surface-pressure compression isotherm experiments using Langmuir monolayers (Figure 8A) have been useful in characterizing interactions among lipids, lipids and fatty acids,[37,40,70−72] and lipids and hydrophilic molecules.[42,61,70] During a surface-pressure compression isotherm experiment, condensing and expanding effects caused by the presence of another lipid (such as MK) can be observed and changes in phase transitions of the lipids can indicate an interaction between the two lipids. To establish that the two MK

DOI: 10.1021/acs.biochem.9b00007
Biochemistry 2019, 58, 1596−1615

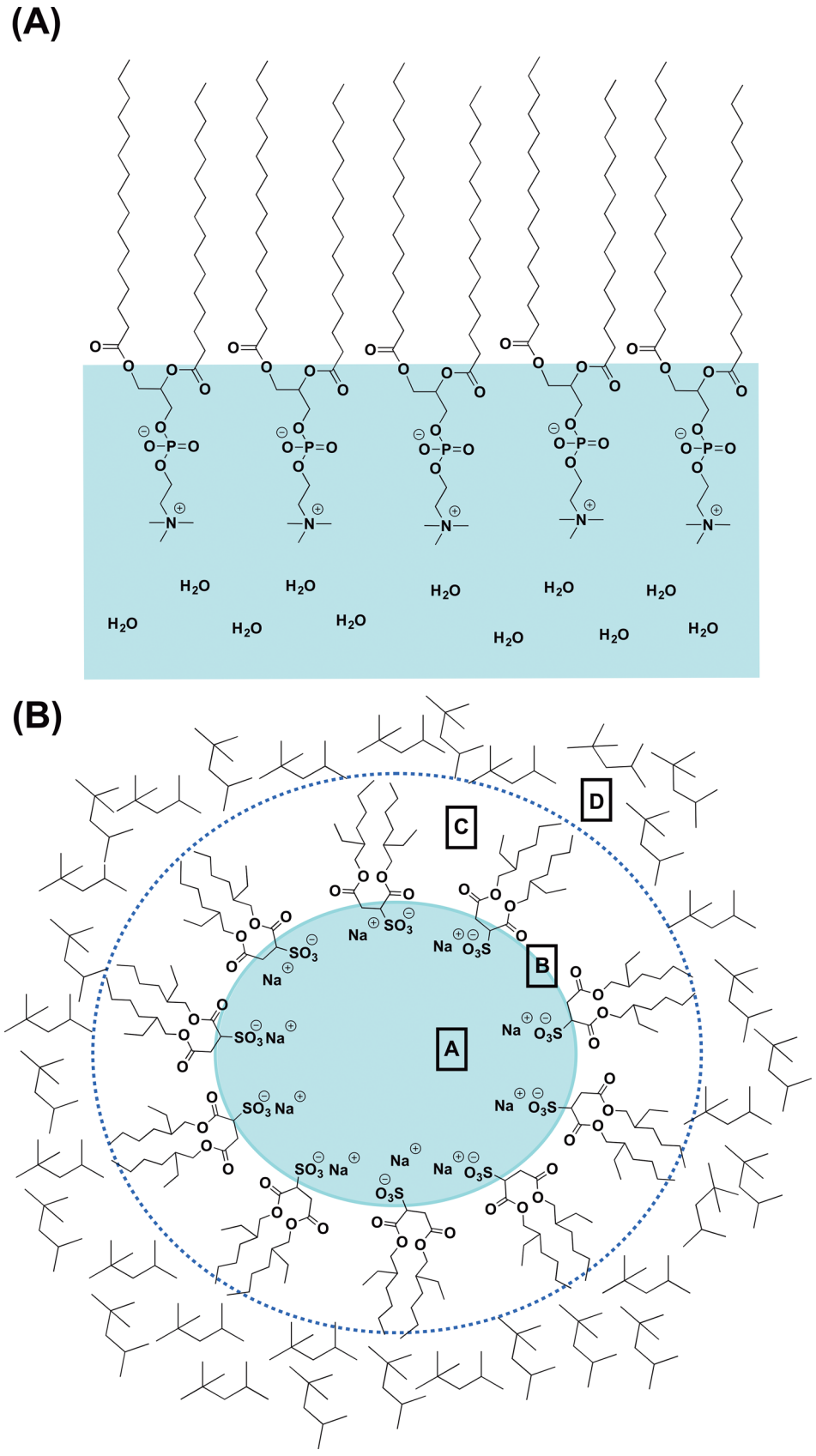

Figure 8. Schematic diagram of (A) a Langmuir phospholipid monolayer (top) and (B) a reverse micelle (bottom) present in a microemulsion with the following labeling: (A) water pool, (B) Stern layer, (C) hydrophobic surfactant tails, and (D) organic solvent isooctane. Adapted with permission from ref 37. Copyright 2018 American Chemical Society.

DOI: 10.1021/acs.biochem.9b00007
Biochemistry 2019, 58, 1596−1615

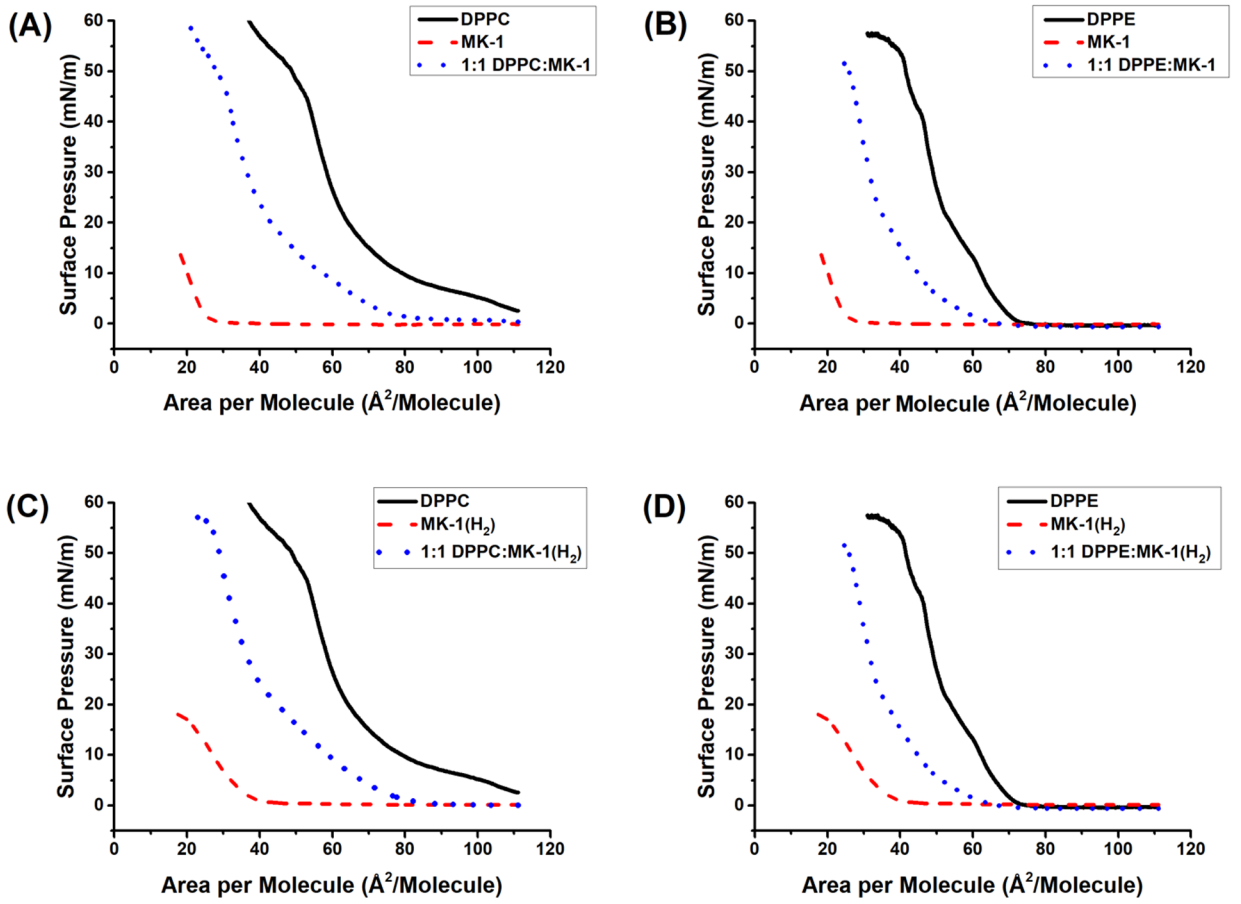

Figure 9. Compression isotherms of MK-1 and MK-1(H_2) films (dashed red lines), DPPC or DPPE phospholipid monolayers (solid black lines), or a 50:50 mixture of MK-1 or MK-1(H_2) and a phospholipid (dotted blue lines): (A) compression isotherms of MK-1 and DPPC, (B) compression isotherms of MK-1 and DPPE, (C) compression isotherms of MK-1(H_2) and DPPC, and (D) compression isotherms of MK-1(H_2) and DPPE.

analogues interact with membrane interfaces, compression isotherms of Langmuir monolayers were used to characterize the interactions of MK-1 and MK-1(H_2) with phospholipid interfaces of common phospholipids found in biological systems such as dipalmitoylphosphatidylcholine (DPPC) or dipalmitoylphosphatidylethanolamine (DPPE).[73−75] Therefore, surface-pressure compression isotherms of Langmuir monolayers consisting of DPPC, DPPE, MK-1, MK-1(H_2), or a mixture of a phospholipid and an MK analogue were performed to determine if the MK analogues had any effect on the packing and compressibility of the phospholipids. The resulting compression isotherms are shown in Figure 9. The control monolayers of DPPC and DPPE are comparable to what has been found in the literature.[40,76] The DPPC monolayers both show a characteristic gas−liquid phase transition at 5 mN/m and collapse at 55 mN/m. The DPPE monolayers also collapsed at 55 mN/m, which aligns well with results in the literature.[40,76]

The MK-1 and MK-1(H_2) pure films were compressed in the same manner as the phospholipid films. Both MK-1 and MK-1(H_2) monolayers did not reach a pressure above 20 mN/m similar to findings reported for ubiquinone-10 (UQ-10) and plastoquinone.[40,71,77] The films were not able to reach a high pressure like other lipoquinones, suggesting that the MK films either slightly soluble in the subphase (similar to UQ-2[40]) as the pressure was increased or aggregation was occurring, which has been shown for lipoquinones with longer isoprenyl side chains.[40,71] Most likely, the MK-1 analogues are aggregating as neither analogue was soluble in D_2O (see 1D ^{1}H NMR RM Spectroscopic Studies).

When the MKs are mixed with DPPC or DPPE phospholipids, differences in phase transitions and compression moduli indicate that an interaction with the MK analogues and phospholipids can be observed. First, the gas to liquid phase transition for DPPC is nonexistent when either MK-1 or MK-1(H_2) is present. This suggests a condensing effect at low pressures. Within all the compression isotherms of the mixed monolayers, a change in slope occurs at ∼20 mN/m [similar to the collapse pressure of MK-1 and MK-1(H_2)], which follows the pattern in the literature with the MK analogues being compressed out of the monolayer to the top of the monolayer similar to UQ.[40,71] To determine if the MK-1 analogues still affected the phospholipid monolayers even at higher surface pressures, the compression moduli of each curve are compared in Figure S29 (see the Supporting Information for compression moduli data and interpretation). In each case, the mixed monolayer exhibited a decrease in its compression modulus (easier to compress) than the pure phospholipid monolayers, indicating that the MK analogues affect the phospholipid monolayer throughout compression even at physiologically relevant surface pressures (∼30−35 mN/m).[41]

Overall, the MK analogues do not form stable monolayers at high pressures (>20 mM/m) and have a compressing effect on the phospholipid monolayers, and at higher pressures, the MK

DOI: 10.1021/acs.biochem.9b00007
Biochemistry 2019, 58, 1596−1615

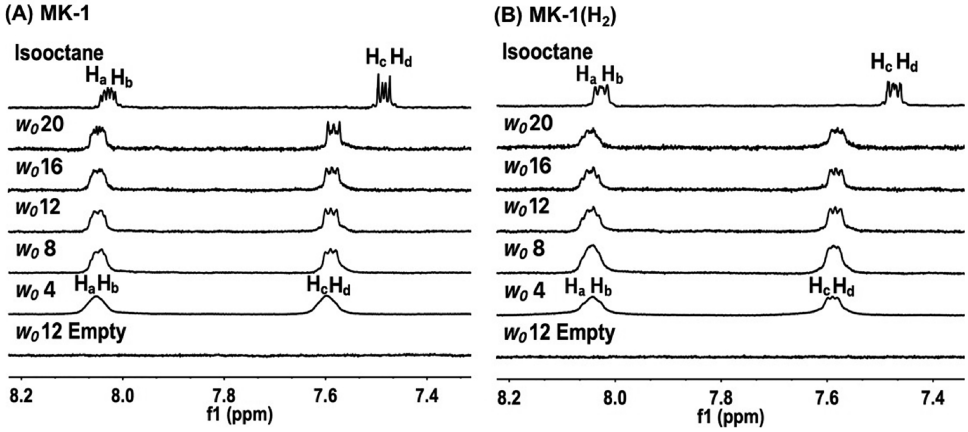

Figure 10. 1D ^{1}H NMR (400 MHz) spectra of (A) MK-1 and (B) MK-1(H_2) aromatic hydrogens H_a, H_b, H_c, and H_d in different sized RMs (w_0 4, 8, 12, 16, and 20) prepared from a 0.50 M AOT/isooctane stock solution. MK-1 or MK-1(H_2) in isooctane is used as a comparison reference spectrum, and w_0 12 Empty is a control spectrum without MK-1 or MK-1(H_2). Peaks are labeled with corresponding hydrogens for MK-1 and MK-1(H_2) (see Figures 3 and 4 for the hydrogen labeling scheme key). Hydrogens, H_a, H_b, H_c, and H_d, undergo a shift upon insertion into the RMs for both MKs. The overall concentrations for the 1.0 mL MK-1 RM samples are as follows: w_0 4, 13.8 mM; w_0 8, 6.5 mM; w_0 12, 3.5 mM; w_0 16, 1.9 mM; w_0 20, 1.3 mM. The overall concentrations for the 1.0 mL MK-1(H_2) RM samples are as follows: w_0 4, 13.8 mM; w_0 8, 6.4 mM; w_0 12, 3.5 mM; w_0 16, 2.0 mM; w_0 20, 1.4 mM.

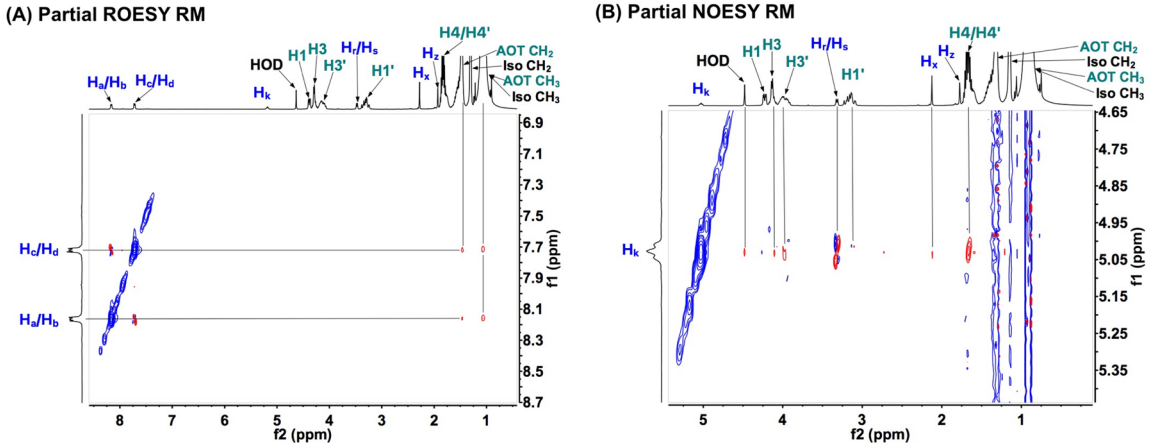

Figure 11. Partial ^{1}H−^{1}H 2D ROESY and ^{1}H−^{1}H 2D NOESY NMR (400 MHz) spectra of MK-1 in a w_0 12 RM. (A) Partial ROESY spectrum illustrating interactions of MK-1 aromatic hydrogens with AOT. (B) Partial NOESY spectrum illustrating interactions of MK-1 H_k hydrogens with AOT. Blue to blue hydrogen text labeling shows MK-1−MK-1 interactions, and blue to teal hydrogen text labeling shows MK-1−AOT interactions. Blue intensity contours represent negative NOEs or ROEs, and red intensity contours represent positive NOEs or ROEs. See Figure 3 for the MK-1 hydrogen labeling scheme key and Figure 13 for the AOT hydrogen labeling scheme key. A standard NOESY pulse sequence consisting of 256 transients with 16 scans in the f1 domain using a 200 ms mixing time and a 1.5 s relaxation delay was used. A standard ROESYAD pulse sequence consisting of 256 transients with 16 scans in the f1 domain using a 200 ms mixing time and a 2.0 s relaxation delay was used.

analogues most likely are compressed out of the monolayer onto the phospholipid tails similar to previously reported lipoquinones with longer isoprenyl side chains.[37,40,71,77] It is important to note that the Langmuir phospholipid monolayers do not provide evidence of a folded MK conformation due to the nature of the experiment; however, they do demonstrate that MK-1 and MK-1(H_2) interact with the phospholipid model membrane interface even at physiological surface pressures like other quinones, and there was not a large difference observed between the unsaturated and saturated MK-1 analogue.[37,40,71,77]

1D ^{1}H NMR Spectroscopic Studies of MK-1 and MK-1(H_2) in RMs. The studies carried out using Langmuir phospholipid monolayers established that the two MKs interacted with the phospholipid interface. However, the placement, orientation, and conformation of the MK-1 analogues within an interface were still uncertain. Therefore, to fully characterize the location, orientation, and conformation of the MKs within a model membrane interface, we used RMs (Figure 8B), which are ternary microemulsion systems in which the surfactant is dissolved in an organic solvent and the addition of water creates nanosized water droplets encased in the surfactant.[44,64−66,78,79] MK-1 or MK-1(H_2) was placed in RMs of various sizes (w_0 4, 8, 12, 16, and 20; where w_0 = [H_2O]/[AOT]), and then 1D ^{1}H NMR spectra were obtained for each RM size as well as a spectrum in isooctane (2,2,4-trimethylpentane) (Figure 10).

The chemical shift difference between MK-1 aromatic hydrogens, H_a/H_b and H_c/H_d, is greater with a value of 0.55 ppm in isooctane versus that of MK-1 in w_0 20 = 0.47 ppm or w_0 4 = 0.45 ppm RMs, which is diagnostic of a change in the environment surrounding MK-1 (Figure 10). Similarly, the chemical shift difference between MK-1(H_2) aromatic hydrogens, H_a/H_b and H_c/H_d, is greater with a value of 0.56 ppm in

DOI: 10.1021/acs.biochem.9b00007
Biochemistry 2019, 58, 1596−1615

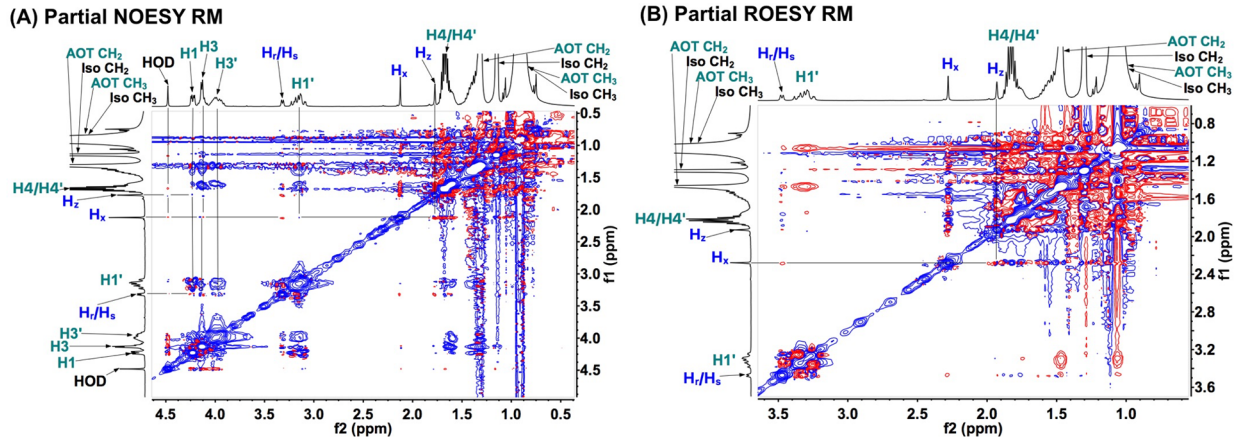

Figure 12. Partial ^{1}H−^{1}H 2D NOESY and ^{1}H−^{1}H 2D ROESY NMR (400 MHz) spectra of MK-1 in a w_0 12 RM. (A) Partial ^{1}H-^{1}H 2D NOESY NMR spectrum in a w_0 12 RM. (B) Partial ^{1}H-^{1}H 2D ROESY NMR spectrum in a w_0 12 RM. Blue to blue hydrogen text labeling shows MK-1−MK-1 interactions, and blue to teal hydrogen text labeling shows MK-1−AOT interactions. Blue intensity contours represent negative NOEs or ROEs, and red intensity contours represent positive NOEs or ROEs. See Figure 3 for the MK-1 hydrogen labeling scheme key and Figure 13 for the AOT hydrogen labeling scheme key. A standard NOESY pulse sequence consisting of 256 transients with 16 scans in the f1 domain using a 200 ms mixing time and a 1.5 s relaxation delay was used. A standard ROESYAD pulse sequence consisting of 256 transients with 16 scans in the f1 domain using a 200 ms mixing time and a 2.0 s relaxation delay was used.

isooctane versus that of MK-1(H_2) in w_0 20 = 0.47 ppm or w_0 4 = 0.45 ppm RMs (Figure 10). The loss of splitting (peak broadening) observed for the aromatic hydrogens as the RM size decreases is attributed to the poorer ability of MK-1 or MK-1(H_2) to tumble freely within the RM interface of smaller sized RMs (e.g., w_0 4). We were unable to obtain a spectrum in D_2O as neither MK was soluble even after extended sonication due to the hydrophobicity of the two MK analogues and it is not likely that either of the MKs are in the water pool due to the very poor water solubility of each compound. Together, the results demonstrated that there was a significant chemical shift difference between the aromatic hydrogens in isooctane and the RMs for both MK-1 analogues. Therefore, we can conclude that neither of the MK-1 analogues are interacting with the isooctane and are residing either at the RM interface or within the AOT alkyl tail region. Furthermore, DLS experiments were carried out and demonstrated that inserting MK-1 or MK-1(H_2) into the RM does not alter the size of the RM or destroy the RMs once inside and the RMs are stable over the course of NMR experiments (see Table S12). Overall, we concluded that MK-1 and MK-1(H_2) interacted with RMs and resided within the RM model membrane interface.

^{1}H−^{1}H 2D NOESY and ^{1}H−^{1}H 2D ROESY NMR Spectroscopic Studies of MK-1 and MK-1(H_2) in a RM Model Membrane System. The 1D ^{1}H NMR spectra of MK-1 and MK-1(H_2) in RMs demonstrated that MK-1 analogues reside within the interface of RMs. However, more information was needed to determine the orientation, position, and conformation while the MK-1 species is residing inside the RM interface. MK-1 was placed inside a w_0 12 RM, and ^{1}H−^{1}H 2D NOESY and ^{1}H−^{1}H 2D ROESY NMR spectra were obtained (Figures 11 and 12 and Figures S12 and S13). NOE/ROE cross peaks between MK-1 and AOT provide evidence for the location, orientation, and conformation within the RM interface. Figure 11A shows ROE cross peaks among all four aromatic hydrogens of MK-1 and the CH_2/CH_3 groups of the AOT alkyl tails. Figure 11B shows cross peaks between MK-1's alkene hydrogen H_k and HOD, H1, H3/H3′, and H4/H4′. Figure 12A also shows cross peaks between hydrogens H_r/H_s and H1, H3, and H3′, which together indicate that MK-1 is located within the RM interface. Panels A and B of Figure 12 show NOE/ROE cross peaks between H_r/H_s and H_z, between H_x and H_z, and between H_z and H1 and H3 and the lack of a cross peak between H_x and H_k, which supports a folded conformation for MK-1 while it is residing in the interface (see Figure S26 for ROE/NOE correlation traces). On the basis of these observations, MK-1 is oriented in a manner in which the naphthoquinone is positioned toward the AOT alkyl tails and the folded isoprenyl side chain is positioned between hydrogens H1/H1′ and H3/H3′ as illustrated in Figure 13. A proposed folded MK-1 conformation that is consistent with the 2D NOESY and ROESY spectral data is illustrated in Figure 14. The phase of the MK-1 to MK-1 cross peaks observed in the NOESY spectrum (Figures 11 and 12) within the RM interface is the opposite phase of the diagonal, indicating MK-1 is behaving as a small molecule within the RM interface and likely tumbling freely but

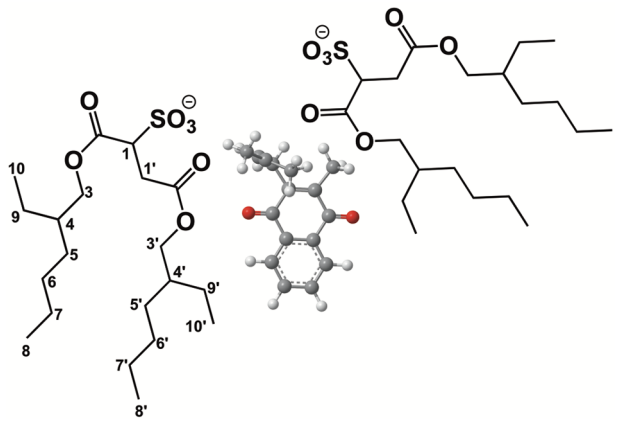

Figure 13. Illustration of the placement and proposed conformation of MK-1 penetrating the RM interface. This arrangement is consistent with the ^{1}H−^{1}H 2D NOESY and ^{1}H−^{1}H 2D ROESY NMR spectral data obtained in a w_0 12 RM. However, MK-1 likely tumbles freely within the interface but maintains interactions with the region of AOT shown in the illustration. The AOT hydrogen labeling scheme key is shown.

DOI: 10.1021/acs.biochem.9b00007
Biochemistry 2019, 58, 1596−1615

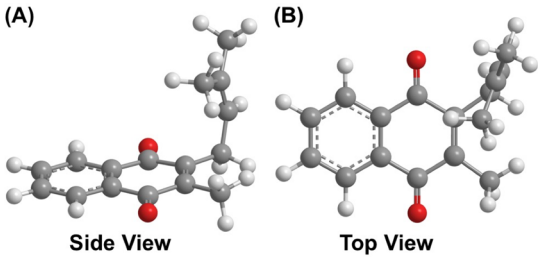

Figure 14. Proposed conformation of MK-1 at an RM interface illustrated using MMFF94 calculations that is consistent with ^{1}H−^{1}H 2D NOESY and ^{1}H−^{1}H 2D ROESY NMR spectral data. (A) Side view of the energy-minimized folded MK-1 conformation (50.3 kcal/mol; H_x−H_z internuclear distance, 2.8 Å). (B) Top view of the energy-minimized proposed MK-1 conformation showing the isoprene methyl groups positioned folded upward.

maintaining interactions with the AOT regions shown in Figure 13.

To determine if saturation of the isoprenyl side chain affects the location and orientation within the RM interface, the same experiment was carried out with MK-1(H_2) (Figure S25). NOE cross peaks are observed between MK-1(H_2) aromatic hydrogens, H_a−H_d, and AOT's CH_2 and CH_3 alkyl tail groups (Figure S25). NOE cross peaks are observed between methylene hydrogens, H_r/H_s, and HOD, H1/H1′, H3/H3′, and H4/H4′. NOE cross peaks are observed between the naphthoquinone methyl, H_x, and HOD, H1/H1′, H3/H3′, and H4/H4′ (Figure S25). The AOT and isooctane hydrogens overlapped with MK-1(H_2)'s terminal methyl hydrogens, H_z and H_y, and the methine hydrogen, H_l, signals in the spectrum for MK-1(H_2) within the RM interface; therefore, we were unable to determine the conformation of MK-1(H_2) within the interface with confidence. Despite this, we would anticipate that MK-1(H_2) adopts a folded conformation similar to that of MK-1 within the RM interface based on similar interactions observed in the 1D and 2D NMR experiments carried out for MK-1. Together, these observations demonstrate that MK-1(H_2) interacted with the interface and has a position and orientation similar to those of MK-1, indicating that saturation of the isoprenyl side chain does induce an observable change in the position and orientation within the RM interface.

Overall, the ^{1}H−^{1}H 2D NOESY and ROESY NMR spectral data of MK-1 inside an RM interface are consistent with MK-1 adopting a folded conformation within an RM model membrane interface. Interestingly, the conformation of MK-1 inside the RM interface remains folded but differs slightly from the folded conformations observed in organic solutions. The observation that MK-1 adopts a folded conformation within the RM model membrane interface is important as understanding the conformational preferences of the first isoprene unit of MK will be crucial in determining and understanding conformations of the naturally occurring longer MK analogues within cellular membranes.

CONCLUSIONS

Lipoquinones such as MK, are special types of lipid-quinones and are essential components of the ETS. Partial saturation of MK in these biological systems is necessary for some organisms to survive such as pathogenic *M. tuberculosis*.[7,8,11] The rationale for the observation of partially saturated MK derivatives in various organisms remains unclear. It is intriguing as the double bonds present in the isoprenyl side chain of MK are not conjugated with each other or to the redox active quinone system and therefore would not be expected to affect the redox potential. Interestingly, we recently showed that MK-2 adopts a folded conformation in which the double bond in the second isoprene unit is in the proximity of the quinone carbonyl groups on the naphthoquinone and may potentially have an influence on the reactivity of the quinone.[37] The studies described herein improve our understanding of the chemical, conformational, and biochemical properties on an important class of quinone-containing compounds involved in electron transfer processes. The partially saturated MKs represent an unrecognized group of biologically significant molecules that are essential for pathogenic taxonomic classification.

In this work, we first demonstrated using a semiquantitative 2D NMR spectroscopy approach that the two simplest, most fundamental MK analogues, unsaturated MK-1 and saturated MK-1(H_2), adopt similar folded−extended conformations in each organic solvent but differ slightly between each organic solvent environment. We also observed that the degree of saturation in the isoprenyl side chain of MK-1 only slightly alters the conformation. Importantly, the conformations observed for MK-1 closely resembled the conformation of the first isoprene unit in MK-2, which we previously showed adopted folded conformations in solution and within a model membrane interface.[37] Together, these results support the first hypothesis that MK-1 analogues adopt folded conformations regardless of the degree of saturation in their isoprenyl side chain.

The quinone redox potentials of MK-1 and MK-1(H_2) were measured in various anhydrous organic solvent environments. The organic solvent environments studied more closely resemble the environment of the cellular membrane in which native MKs are located and serve as better comparisons for biological reactivity than those carried out in aqueous solutions. We demonstrated that the measured quinone redox potentials of MK-1 and MK-1(H_2) varied with the solvent environment (presumably mainly due to differences in dielectric constants) where the ease of quinone reduction for the $Q/Q^{\bullet-}$ process follows the trend DMSO > ACN > pyridine. Remarkably, we report for the first time that the degree of saturation in the isoprenyl side chain of MK-1 influences the observed quinone redox potential, where unsaturation in the isoprenyl side chain of MK-1 makes the quinone easier to reduce by ∼20 mV and the difference is conserved across several organic solvents (pyridine, ACN, and DMSO). The observed ∼20 mV redox potential difference is presumably due mostly to a perturbation of the electronics of the quinone system upon saturation of the double bond by an indirect through-bond effect. The observation of a 20 mV difference in the redox potential between the two MK-1 derivatives with a saturated and unsaturated isoprenyl side chain observed in three different solvents is unexpected and may reflect some important general reactivity pattern of this system. We speculate that if such a difference is also observed for the MKs with longer isoprenyl side chains that it may reflect the biological function of these molecules and provide evidence for the possibility that such a small difference in redox potential may be biologically significant. However, in the simple MK-1 system containing one isoprene unit, the side chain may not have the spatial reach needed present in the MK-9 system, and therefore, more data are needed to properly evaluate the longer MK derivatives. The electrochemical results

DOI: 10.1021/acs.biochem.9b00007
Biochemistry 2019, 58, 1596−1615

confirm our second hypothesis that saturation of the isoprenyl side chain of MK-1 affects the observed quinone redox potential.

Finally, combining results, we found MK-1 and MK-1(H_2) both interacted with Langmuir phospholipid monolayers and RM model membrane interfaces, where MK-1 and MK-1(H_2) had very similar interactions with the Langmuir phospholipid monolayers (DPPC and DPPE phospholipids) and similar placement and location within the RM interface. Importantly, MK-1 also adopted a folded conformation within the RM model membrane interface, further supporting our first hypothesis. The results combined from all the conformational analysis studies presented herein for MK-1 and MK-1(H_2) indicated a folded−extended conformation to be a favorable and stable conformation for MK-1 analogues. Altogether, these results are significant as the conformation and reactivity of these MKs in organic solution and model membrane interfaces provide a first prediction/consideration of the form that exists within the native hydrophobic cellular membrane interface.

Overall, the findings of this study improve our understanding of how the conformation and the degree of saturation in the isoprenyl side chain affect the reactivity and function of biologically relevant molecules. The elucidation of the conformation of MK-1 and MK-1(H_2) in organic solutions and at a model membrane interface is essential and necessary as understanding the conformational preferences of the first isoprene unit of MK is useful for predicting the conformations of the naturally occurring longer MK analogues within solution and cellular membranes. We observed that partial saturation in the isoprenyl side chain only minimally alters the conformation of MK-1 but may potentially affect the reactivity and function within biologically relevant environments because a difference in the redox potential is observed. MK analogues with longer isoprenyl side chains (e.g., MK-9) may also adopt folded conformations, although likely much more complex. Saturation of the double bond in the first isoprene unit of the isoprenyl side chain serves to only minimally alter the preferred conformation but distinctly affects the redox function. The results presented here provide a working model involving the role of structure and redox potential that explains why partial saturation of MK is a virulence factor for pathogenic *M. tuberculosis*, which is responsible for the deaths of ∼1.3 million people annually.[7,8,80]

■ ASSOCIATED CONTENT

Supporting Information

The Supporting Information is available free of charge on the ACS Publications website at DOI: 10.1021/acs.biochem.9b00007.

General experimental information, 1D and 2D NMR spectroscopic and structural data for MK-1 and MK-1(H_2), MK-1 and MK-1(H_2) conformations and conformational analysis and tables of relevant internuclear hydrogen distances, energies, and Cartesian coordinates, electrochemistry methods and data and discussion, ^{1}H NMR spectra of MK-1 with TBAP, Langmuir monolayer compression moduli of MK-1 and MK-1(H_2) and interpretation, and DLS data and interpretation (PDF)

■ AUTHOR INFORMATION

Corresponding Author

*E-mail: Debbie.Crans@colostate.edu.

ORCID

Jordan T. Koehn: 0000-0003-3008-6303
Benjamin J. Peters: 0000-0002-6219-4897
Cameron Van Cleave: 0000-0002-0924-1738
Dean C. Crick: 0000-0001-9281-7058
Debbie C. Crans: 0000-0001-7792-3450

Funding

D. C. Crans and D. C. Crick thank the National Institutes of Health (Grant AI119567) and the National Science Foundation (Grant CHE-1709564) for funding. D. C. Crans also thanks the Arthur Cope Foundation administered by the American Chemical Society for partial support.

Notes

The authors declare no competing financial interest.

■ ACKNOWLEDGMENTS

The authors thank Dr. Christopher Rithner for assistance with NMR spectroscopy and Taylor Lucia and Lining Yang for early contributions to this project.

■ REFERENCES

(1) Aguilar-Martínez, M., Macías-Ruvalcaba, N. A., Bautista-Martínez, J. A., Gómez, M., González, F. J., and González, I. (2004) Review: Hydrogen Bond and Protonation as Modifying Factors of the Quinone Reactivity. *Curr. Org. Chem. 8*, 1721−1738.

(2) Astudillo-Sánchez, P. D., Morales-Martínez, D., Sánchez, A., Rocha-Ortiz, G., and Salas-Reyes, M. (2017) Electrochemical Study of the Interactions Between Anionic Species of Menadione and Alkylated Nucleobases in Dimethylsulfoxide. *J. Electroanal. Chem. 801*, 104−113.

(3) Gunner, M. R., Madeo, J., and Zhu, Z. (2008) Modification of Quinone Electrochemistry by the Proteins in the Biological Electron Transfer Chains: Examples from Photosynthetic Reaction Centers. *J. Bioenerg. Biomembr. 40* (5), 509−519.

(4) Monks, T. J., Hanzlik, R. P., Cohen, G. M., Ross, D., and Graham, D. G. (1992) Quinone Chemistry and Toxicity. *Toxicol. Appl. Pharmacol. 112* (1), 2−16.

(5) Abraham, I., Joshi, R., Pardasani, P., and Pardasani, R. T. (2011) Recent Advances in 1,4-Benzoquinone Chemistry. *J. Braz. Chem. Soc. 22* (3), 385−421.

(6) Nowicka, B., and Kruk, J. (2010) Occurrence, Biosynthesis and Function of Isoprenoid Quinones. *Biochim. Biophys. Acta, Bioenerg. 1797*, 1587−1605.

(7) Upadhyay, A., Fontes, F. L., Gonzalez-Juarrero, M., McNeil, M. R., Crans, D. C., Jackson, M., and Crick, D. C. (2015) Partial Saturation of Menaquinone in *Mycobacterium tuberculosis*: Function and Essentiality of a Novel Reductase, MenJ. *ACS Cent. Sci. 1* (6), 292−302.

(8) Upadhyay, A., Kumar, S., Rooker, S. A., Koehn, J. T., Crans, D. C., McNeil, M. R., Lott, J. S., and Crick, D. C. (2018) Mycobacterial MenJ: An Oxidoreductase Involved in Menaquinone Biosynthesis. *ACS Chem. Biol. 13*, 2498−2507.

(9) da Costa, M. S., Albuquerque, L., Nobre, M. F., and Wait, R. (2011) The Extraction and Identification of Respiratory Lipoquinones of Prokaryotes and Their Use in Taxonomy. In *Methods in Microbiology, Vol 38: Taxonomy of Prokaryotes* (Rainey, F., and Oren, A., Eds.) Vol. *38*, pp 197−206, Elsevier Academic Press Inc., San Diego.

(10) Kroppenstedt, R. M., and Mannheim, W. (1989) Lipoquinones in Members of the Family Pasteurellaceae. *Int. J. Syst. Bacteriol. 39* (3), 304−308.

DOI: 10.1021/acs.biochem.9b00007
Biochemistry 2019, 58, 1596−1615

(11) Collins, M. D., and Jones, D. (1981) Distribution of Isoprenoid Quinone Structural Types in Bacteria and Their Taxonomic Implications. *Microbiol. Rev. 45* (2), 316−354.
(12) Meganathan, R. (2001) Biosynthesis of Menaquinone (Vitamin K_2) and Ubiquinone (Coenzyme Q): A Perspective on Enzymatic Mechanisms. *Vitam. Horm. 61*, 173−218.
(13) Jarchow-Choy, S. K., Koppisch, A. T., and Fox, D. T. (2014) Synthetic Routes to Methylerythritol Phosphate Pathway Intermediates and Downstream Isoprenoids. *Curr. Org. Chem. 18*, 1050−1072.
(14) Collins, M. D., Shah, H. N., and Minnikin, D. E. (1980) A Note on the Separation of Natural Mixtures of Bacterial Menaquinones Using Reverse-phase Thin-layer Chromatography. *J. Appl. Bacteriol. 48* (2), 277−282.
(15) Thomson, R. H. (1971) *Naturally Occurring Quinones*, Academic Press Inc.
(16) Kurosu, M., and Begari, E. (2010) Vitamin K_2 in Electron Transport System: Are Enzymes Involved in Vitamin K_2 Biosynthesis Promising Drug Targets? *Molecules 15* (3), 1531−1553.
(17) Nakagawa, K., Hirota, Y., Sawada, N., Yuge, N., Watanabe, M., Uchino, Y., Okuda, N., Shimomura, Y., Suhara, Y., and Okano, T. (2010) Identification of UBIAD1 as a Novel Human Menaquinone-4 Biosynthetic Enzyme. *Nature 468*, 117−121.
(18) Vos, M., Esposito, G., Edirisinghe, J. N., Vilain, S., Haddad, D. M., Slabbaert, J. R., Van Meensel, S., Schaap, O., De Strooper, B., Meganathan, R., Morais, V. A., and Verstreken, P. (2012) Vitamin K_2 Is a Mitochondrial Electron Carrier That Rescues Pink1 Deficiency. *Science 336*, 1306−1310.
(19) Josey, B. J., Inks, E. S., Wen, X., and Chou, C. J. (2013) Structure−Activity Relationship Study of Vitamin K Derivatives Yields Highly Potent Neuroprotective Agents. *J. Med. Chem. 56*, 1007−1022.
(20) Rahn, J. J., Bestman, J. E., Josey, B. J., Inks, E. S., Stackley, K. D., Rogers, C. E., Chou, C. J., and Chan, S. S. L. (2014) Novel Vitamin K Analogs Suppress Seizures in Zebrafish and Mouse Models of Epilepsy. *Neuroscience 259*, 142−154.
(21) Chadar, D., Camilles, M., Patil, R., Khan, A., Weyhermuller, T., and Salunke-Gawali, S. (2015) Synthesis and Characterization of *n*-alkylamino Derivatives of Vitamin K3: Molecular Structure of 2-propylamino-3-methyl-1,4-naphthoquinone and Antibacterial Activities. *J. Mol. Struct. 1086*, 179−189.
(22) Kathawate, L., Joshi, P. V., Dash, T. K., Pal, S., Nikalje, M., Weyhermuller, T., Puranik, V. G., Konkimalla, V. B., and Salunke-Gawali, S. (2014) Reaction Between Lawsone and Aminophenol Derivatives: Synthesis, Characterization, Molecular Structures and Antiproliferative Activity. *J. Mol. Struct. 1075*, 397−405.
(23) Klauda, J. B., Brooks, B. R., MacKerell, A. D., Venable, R. M., and Pastor, R. W. (2005) An Ab Initio Study on the Torsional Surface of Alkanes and Its Effect on Molecular Simulations of Alkanes and a DPPC Bilayer. *J. Phys. Chem. B 109*, 5300−5311.
(24) Woodward, R. B., and Bloch, K. (1953) The Cyclization of Squalene in Cholesterol Synthesis. *J. Am. Chem. Soc. 75*, 2023−2024.
(25) Chum, S. P., Knight, G. W., Ruiz, J. M., and Phillips, P. J. (1994) Computer Modeling of {110} Adjacent Reentry of Polyethylene Molecules. *Macromolecules 27*, 656−659.
(26) Robertson, M. B., Klein, P. G., Ward, I. M., and Packer, K. J. (2001) NMR Study of the Energy Difference and Population of the *gauche* and *trans* Conformations in Solid Polyethylene. *Polymer 42*, 1261−1264.
(27) Nikki, K., Inakura, H., Wu-Le, Suzuki, N., and Endo, T. (2001) Remarkable Changes in Conformations of *n*-alkanes with thier Carbon Numbers and Aromatic Solvents. *J. Chem. Soc., Perkin Trans. 2*, 2370−2373.
(28) Nikki, K., and Nakagawa, N. (1983) Elucidation of the Structure of Alkane Chains in Solution by Means of ^{1}H NMR. *Org. Magn. Reson. 21* (9), 552−554.
(29) Nikki, K. (1990) ^{1}H and ^{13}C NMR Aromatic Solvent-induced Shifts of *n*-alkanes. *Magn. Reson. Chem. 28* (5), 385−388.
(30) Schramm, M. P., and Rebek, J., Jr. (2006) Moving Targets: Recognition of Alkyl Groups. *Chem. - Eur. J. 12*, 5924−5933.
(31) Choudhury, R., Barman, A., Prabhakar, R., and Ramamurthy, V. (2013) Hydrocarbons Depending on the Chain Length and Head Group Adopt Different Conformations within a Water-Soluble Nanocapsule: ^{1}H NMR and Molecular Dynamics Studies. *J. Phys. Chem. B 117*, 398−407.
(32) Ko, Y. H., Kim, Y., Kim, H., and Kim, K. (2011) U-Shaped Conformation of Alkyl Chains Bound to a Synthetic Receptor Cucurbit[8]uril. *Chem. - Asian J. 6*, 652−657.
(33) Ko, Y. H., Kim, H., Kim, Y., and Kim, K. (2008) U-Shaped Conformation of Alkyl Chain Bound to a Synthetic Host. *Angew. Chem., Int. Ed. 47*, 4106−4109.
(34) Zakharov, A. V., and Vogt, N. (2011) Conformational Analysis of Vitamin K_1 Model Molecule: A Theoretical Study. *Struct. Chem. 22* (2), 305−311.
(35) Tynkkynen, T., Hassinen, T., Tiainen, M., Soininen, P., and Laatikainen, R. (2012) ^{1}H NMR Spectral Analysis and Conformational Behavior of *n*-alkanes in Different Chemical. *Magn. Reson. Chem. 50*, 598−607.
(36) Ishihara, M., and Sakagami, H. (2007) QSAR of Molecular Structure and Cytotoxic Activity of Vitamin K_2 Derivatives with Concept of Absolute Hardness. *Anticancer Res. 27*, 4059−4063.
(37) Koehn, J. T., Magallanes, E. S., Peters, B. J., Beuning, C. N., Haase, A. A., Zhu, M. J., Rithner, C. D., Crick, D. C., and Crans, D. C. (2018) A Synthetic Isoprenoid Lipoquinone, Menaquinone-2, Adopts a Folded Conformation in Solution and at a Model Membrane Interface. *J. Org. Chem. 83*, 275−288.
(38) Stahla, M. L., Baruah, B., James, D. M., Johnson, M. D., Levinger, N. E., and Crans, D. C. (2008) ^{1}H NMR Studies of Aerosol-OT Reverse Micelles with Alkali and Magnesium Counterions: Preparation and Analysis of MAOTs. *Langmuir 24* (12), 6027−6035.
(39) Samart, N., Beuning, C. N., Haller, K. J., Rithner, C. D., and Crans, D. C. (2014) Interaction of a Biguanide Compound with Membrane Model Interface Systems: Probing the Properties of Antimalaria and Antidiabetic Compounds. *Langmuir 30* (29), 8697−8706.
(40) Quinn, P. J., and Esfahani, M. A. (1980) Ubiquinones have Surface-Active Properties Suited to Transport Electrons and Protons Across Membranes. *Biochem. J. 185*, 715−722.
(41) Jones, M. N., and Chapman, D. (1995) *Micelles, Monolayers, and Biomembranes*, Wiley-Liss, New York.
(42) Peters, B. J., Groninger, A. S., Fontes, F. L., Crick, D. C., and Crans, D. C. (2016) Differences in Interactions of Benzoic Acid and Benzoate with Interfaces. *Langmuir 32* (37), 9451−9459.
(43) Peters, B. J., Van Cleave, C., Haase, A. A., Hough, J. P. B., Giffen-Kent, K. A., Cardiff, G. M., Sostarecz, A. G., Crick, D. C., and Crans, D. C. (2018) Structure Dependence of Pyridine and Benzene Derivatives on Interactions with Model Membranes. *Langmuir 34*, 8939−8951.
(44) Maitra, A. (1984) Determination of Size Parameters of Water-aerosol-OT Oil Reverse Micelles From Their Nuclear Magnetic-resonance Data. *J. Phys. Chem. 88* (21), 5122−5125.
(45) Hagiwara, E., Hatanaka, Y., Gohda, K.-i., and Hiyama, T. (1995) Allylation of Quinones with Allyl(trifluoro)silanes: Direct Synthesis of Isoprenoid Quinones. *Tetrahedron Lett. 36* (16), 2773−2776.
(46) Mal, D., Ghosh, K., and Jana, S. (2015) Synthesis of Vitamin K and Related Naphthoquinones via Demethoxycarbonylative Annulations and a Retro-Wittig Rearrangement. *Org. Lett. 17*, 5800−5803.
(47) Teitelbaum, A. M., Scian, M., Nelson, W. L., and Rettie, A. E. (2015) Efficient Syntheses of Vitamin K Chain-Shortened Acid Metabolites. *Synthesis 47*, 944−948.
(48) Yamago, S., Hashidume, M., and Yoshida, J.-i. (2002) A New Synthetic Route to Substituted Quinones by Radical-mediated Coupling of Organotellurium Compounds with Quinones. *Tetrahedron 58*, 6805−6813.
(49) Daines, A. M., Payne, R. J., Humphries, M. E., and Abell, A. D. (2003) The Synthesis of Naturally Occurring Vitamin K and Vitamin K Analogues. *Curr. Org. Chem. 7*, 1625−1634.

DOI: 10.1021/acs.biochem.9b00007
Biochemistry 2019, 58, 1596−1615

(50) Payne, R. J., Daines, A. M., Clark, B. M., and Abell, A. D. (2004) Synthesis and Protein Conjugation Studies of Vitamin K Analogues. *Bioorg. Med. Chem. 12* (22), 5785−5791.
(51) Suhara, Y., Wada, A., Tachibana, Y., Watanabe, M., Nakamura, K., Nakagawa, K., and Okano, T. (2010) Structure-activity Relationships in the Conversion of Vitamin K Analogues into Menaquinone-4. Substrates Essential to the Synthesis of Menaquinone-4 in Cultured Human Cell Lines. *Bioorg. Med. Chem. 18* (9), 3116−3124.
(52) Coppa, F., Fontana, F., Minisci, F., Nogueira Barbosa, M. C., and Vismara, E. (1991) Homolytic Alkylation of Naphthoquinone and Methyl-naphthoquinone. Enthalpic, Steric and Polar Effects. *Tetrahedron 47* (35), 7343−7352.
(53) Koehn, J. T., Crick, D. C., and Crans, D. C. (2018) Synthesis and Characterization of Partially and Fully Saturated Menaquinone Derivatives. *ACS Omega 3*, 14889−14901.
(54) Jones, C. R., Butts, C. P., and Harvey, J. N. (2011) Accuracy in Determining Interproton Distances using Nuclear Overhauser Effect Data from a Flexible Molecule. *Beilstein J. Org. Chem. 7*, 145−150.
(55) Cooper, G. M., and Hausman, R. E. (2009) *The Cell: A Molecular Approach*, 5th ed., p 820, Sinauer Associates, Inc., Sunderland, MA.
(56) Nelson, D. L., and Cox, M. M. (2008) *Lehninger Principles of Biochemistry*, 5th ed., p 1158, W. H. Freeman and Co., New York.
(57) Dryhurst, G., Kadish, K. M., Scheller, F., and Renneberg, R. (1982) *Biological Eletrochemistry*, Academic Press, New York.
(58) Wawzonek, S., Berkey, R., Blaha, E. W., and Runner, M. E. (1956) Polarographic Studies in Acetonitrile and Dimethylformamide: III. Behavior of Quinones and Hydroquinones. *J. Electrochem. Soc. 103* (8), 456−459.
(59) Jaworski, J. S., Leniewska, E., and Kalinowski, M. K. (1979) Solvent Effect on the Redox Potential of Quinone-semiquinone Systems. *J. Electroanal. Chem. Interfacial Electrochem. 105* (2), 329−334.
(60) Prince, R. C., Leslie Dutton, P., and Malcolm Bruce, J. (1983) Electrochemistry of Ubiquinones. *FEBS Lett. 160* (1), 273−276.
(61) Sostarecz, A. G., Gaidamauskas, E., Distin, S., Bonetti, S. J., Levinger, N. E., and Crans, D. C. (2014) Correlation of Insulin-Enhancing Properties of Vanadium-Dipicolinate Complexes in Model Membrane Systems: Phospholipid Langmuir Monolayers and AOT Reverse Micelles. *Chem. - Eur. J. 20* (17), 5149−5159.
(62) Riter, R. E., Kimmel, J. R., Undiks, E. P., and Levinger, N. E. (1997) Novel Reverse Micelles Partitioning Nonaqueous Polar Solvents in a Hydrocarbon Continuous Phase. *J. Phys. Chem. B 101* (41), 8292−8297.
(63) Durantini, A. M., Falcone, R. D., Silber, J. J., and Correa, N. M. (2016) Effect of Confinement on the Properties of Sequestered Mixed Polar Solvents: Enzymatic Catalysis in Nonaqueous 1,4-Bis-2-ethylhexylsulfosuccinate Reverse Micelles. *ChemPhysChem 17* (11), 1678−1685.
(64) Lepori, C. M. O., Correa, N. M., Silber, J. J., and Falcone, R. D. (2016) How the Cation 1-butyl-3-methylimidazolium Impacts the Interaction Between the Entrapped Water and the Reverse Micelle Interface Created with an Ionic Liquid-like Surfactant. *Soft Matter 12* (3), 830−844.
(65) Baruah, B., Roden, J. M., Sedgwick, M., Correa, N. M., Crans, D. C., and Levinger, N. E. (2006) When Is Water Not Water? Exploring Water Confined in Large Reverse Micelles Using a Highly Charged Inorganic Molecular Probe. *J. Am. Chem. Soc. 128*, 12758−12765.
(66) Odella, E., Falcone, R. D., Silber, J. J., and Correa, N. M. (2016) Nanoscale Control Over Interfacial Properties in Mixed Reverse Micelles Formulated by Using Sodium 1,4-bis-2-ethylhexylsulfosuccinate and Tri-n-octyl Phosphine Oxide Surfactants. *ChemPhysChem 17* (15), 2407−2414.
(67) Diaz-Fernandez, Y., Foti, F., Mangano, C., Pallavicini, P., Patroni, S., Perez-Gramatges, A., and Rodriguez-Calvo, S. (2006) Micelles for the Self-Assembly of "Off−On−Off" Fluorescent Sensors for pH Windows. *Chem. - Eur. J. 12*, 921−930.
(68) Pallavicini, P., Diaz-Fernandez, Y., and Pasotti, L. (2009) Micelles as Nanosized Containers for the Self-assembly of Multicomponent Fluorescent Sensors. *Coord. Chem. Rev. 253*, 2226−2240.
(69) Stefaniu, C., Brezesinski, G., and Mohwald, H. (2014) Langmuir Monolayers as Models to Study Processes at Membrane Surfaces. *Adv. Colloid Interface Sci. 208*, 197−213.
(70) Choi, Y., Attwood, S. J., Hoopes, M. I., Drolle, E., Karttunen, M., and Leonenko, Z. (2014) Melatonin Directly Interacts with Cholesterol and Alleviates Cholesterol Effects in Dipalmitoylphosphatidylcholine Monolayers. *Soft Matter 10*, 206−213.
(71) Hoyo, J., Torrent-Burgues, J., and Guaus, E. (2012) Biomimetic Monolayer Films of Monogalactosyldiacylglycerol Incorporating Ubiquinone. *J. Colloid Interface Sci. 384*, 189−197.
(72) Panda, A. K., Nag, K., Harbottle, R. R., Possmayer, F., and Petersen, N. O. (2004) Thermodynamic Studies on Mixed Molecular Langmuir Films: Part 2. Mutual Mixing of DPPC and Bovine Lung Surfactant Extract with Long-chain Fatty Acids. *Colloids Surf., A 247* (1), 9−17.
(73) Veldhuizen, E. J. A., Batenburg, J. J., van Golde, L. M. G., and Haagsman, H. P. (2000) The Role of Surfactant Proteins in DPPC Enrichment of Surface Films. *Biophys. J. 79*, 3164−3171.
(74) Wustneck, R., Perez-Gil, J., Wustneck, N., Cruz, A., Fainerman, V. B., and Pison, U. (2005) Interfacial Properties of Pulmonary Surfactant Layers. *Adv. Colloid Interface Sci. 117* (1), 33−58.
(75) Sohlenkamp, C., and Geiger, O. (2016) Bacterial Membrane Lipids: Diversity in Structures and Pathways. *FEMS Microbiol. Rev. 40* (1), 133−159.
(76) Toimil, P., Prieto, G., Minones, J., Jr, and Sarmiento, F. (2010) A Comparative Study of F-DPPC/DPPC Mixed Monolayers. Influence of Subphase Temperature on F-DPPC and DPPC Monolayers. *Phys. Chem. Chem. Phys. 12*, 13323−13332.
(77) Hoyo, J., Guaus, E., Torrent-Burgues, J., and Sanz, F. (2015) Biomimetic Monolayer Films of Digalactosyldiacylglycerol Incorporating Plastoquinone. *Biochim. Biophys. Acta, Biomembr. 1848* (6), 1341−1351.
(78) Sedgwick, M. A., Trujillo, A. M., Hendricks, N., Levinger, N. E., and Crans, D. C. (2011) Coexisting Aggregates in Mixed Aerosol OT and Cholesterol Microemulsions. *Langmuir 27* (3), 948−954.
(79) Zan, G. T., and Wu, Q. S. (2016) Biomimetic and Bioinspired Synthesis of Nanomaterials/Nanostructures. *Adv. Mater. 28* (11), 2099−2147.
(80) Glaziou, P., Sismanidis, C., Floyd, K., and Raviglione, M. (2015) Global Epidemiology of tuberculosis. *Cold Spring Harbor Perspect. Med. 5*, a017798.

DOI: 10.1021/acs.biochem.9b00007
Biochemistry 2019, 58, 1596−1615